

SUPER RESOLUTION MICROSCOPY OF LIPID BILAYER PHASES AND SINGLE
MOLECULE KINETIC STUDIES ON MEROCYANINE 540 BOUND LIPID
VESICLES.

Chin-Kuei Kuo

A DISSERTATION

in

Chemistry

Presented to the Faculties of the University of Pennsylvania in
Partial Fulfillment of the Requirements for the Degree of Doctor of Philosophy
2012

Professor Robin M. Hochstrasser
Supervisor of Dissertation

Professor Gary Molander
Graduate Group Chair

Dissertation Committee

Christopher B. Murray, Professor of Chemistry
Tobias Baumgart, Associate Professor of Chemistry
Ivan J. Dmochowski, Associate Professor of Chemistry

SUPER RESOLUTION MICROSCOPY OF LIPID BILAYER PHASES AND SINGLE
MOLECULE KINETIC STUDIES ON MEROCYANINE 540 BOUND LIPID
VESICLES.

COPYRIGHT

2012

Chinkuei Kuo

ABSTRACT

SUPER RESOLUTION MICROSCOPY OF LIPID BILAYER PHASES AND SINGLE MOLECULE KINETIC STUDIES ON MEROCYANINE 540 BOUND LIPID VESICLES.

Chinkuei Kuo

Robin M. Hochstrasser

Recently, observing biological process and structural details in live cell became feasible after the introduction of super-resolution microscopy. Super-resolution microscopy by single molecule localization is the method that has commonly been used for such purpose. There are mainly three approaches to it: stochastic optical reconstruction microscopy (STORM), photoactivated localization microscopy (PALM), and point accumulation in nanoscale topology (PAINT). STORM and PALM rely on external laser control and use of photoactivable fluorescent protein or photoswitchable dyes and are technically challenging. The PAINT method relies on the control of thermal reaction rates to enable the switching between bright and dark states. Therefore, many conventional fluorescent probes can be applied in PAINT method and the images denote

different information composed of interactions between the probe and its immediate environment by variations of probe parameters.

The existence of lipid rafts has been under debates for decades due to the lack of a tool to directly visualize them in live cells. In the thesis, we combine PAINT with a phase sensitive dye, Merocyanine 540, to enable nanoscale observation of phase separation on supported lipid bilayers of mixed liquid/gel phases. The imaging results are presented in the chapter 3. Given that this is the first example of visualization of nanoscale phase separation of lipid bilayers using an optical microscope, we further looked into the kinetics of MC540 monomer dimer equilibrium in lipid bilayers using single molecule intensity time trajectory analysis and polarization dependent imaging. Our finding confirms that perpendicular monomeric MC540 (to the membrane surface) is the emitting species in our system and it stays fluorescent for roughly 3 ms before it switches off to dark states. This part of analysis is presented in the chapter 4. All the materials, procedures to carry out experiments and data analysis, methods involved in our study are briefed in the chapter 2. It was shown that the PAINT method of super-resolution imaging using the dye MC540 is useful for imaging nanoscale phase domains in binary lipid bilayers. The extension of our approach to other binary or ternary lipid model or natural systems provides a promising new super-resolution strategy.

TABLE OF CONTENTS

Title	i
Copyright	ii
Abstract	iii
Table of Contents	iv
List of Schemes	v
List of Figures	vi
Chapter 1	Introduction.....	1
Chapter 2	Experimental overview.....	25
Chapter 3	Super resolution microscopy of lipid bilayer phases.....	43
Chapter 4	Monomer-dimer equilibrium of merocyanine 540 probed by single molecule kinetic studies.....	64
Chapter 5	Conclusion.....	114

LIST OF SCHEMES

Scheme 2.1	The experiment setup of the single molecule confocal microscopy.....	40
Scheme 2.2	A simplified intensity time trajectory from a two-state system.....	41
Scheme 2.3	Molecular structure of merocyanine 540.....	42
Scheme 3.1	Kinetic scheme for the dimerization of MC540 in liposomes.....	56
Scheme 4.1	Proposed kinetic schemes for the fluorescence intermittency of MC540 bound vesicles.....	102
Scheme 4.2	Illustration of distribution of MC540 in lipid bilayers.....	103

LIST OF FIGURES

Figure 3.1	Fluorescence spectra of MC540 in supported lipid bilayers.....	57
Figure 3.2	Comparison of populations of fluorescent monomers in the liquid and gel phase in supported lipid bilayers.....	58
Figure 3.3	Comparison of PAINT and TIRFM images.....	60
Figure 3.4	Comparison of Nile Red and MC540 super-resolution images.....	62
Figure 4.1	Fluorescence images of MC540 bound vesicles on a glass surface.....	104
Figure 4.2	Fluorescence spectra of MC540 bound vesicles on a glass surface.....	105
Figure 4.3	Fluorescence intensity-time trajectory on a MC540 bound DMPC vesicle.....	106
Figure 4.4	Probability distributions of the width of fluorescence bursts and dark periods from over 250 MC540 bound vesicles.....	107
Figure 4.5	Mean on time and off time rate for vesicles of different lipid.....	109
Figure 4.6	Simulated off-time probability distribution function and predicted average off-time versus amount of MC540 in bilayers.....	110
Figure 4.7	Polarization dependent PAINT image of a nanosized lipid bilayer wrapped silica and number density distribution of it under various polarization conditions.....	111
Figure 4.8	Polarization dependent fluorescence image of DLPC GUVs.....	113

Chapter 1 Introduction

Fluorescence spectroscopy and microscopy have been useful and common tools for the scientific community to tackle biological problems. It has even escalated to another level since single molecule observations become possible since two decades ago¹⁻⁵. The combination of the unique ability for light to penetrate through biological samples (cells, tissues, and e.t.c.) and the ability to gather information from individual single molecules (enzymes, RNA, DNA, functional proteins, and etc.) has proven flourishing to dissect important tangling biological issues⁶⁻⁹, not only in vitro but also in vivo. However, the optical method has still been limited by diffraction. Yet this has changed as the introduction of super-resolution microscopy to enable us to observe things optically at a resolution that is beyond the diffraction limit came along in 2006¹⁰. Surprisingly biological details and images^{10, 11} have been stacking since then. Interesting biological problems that occur at spatial scale below 300 nm now are to be answered with the newly developed tool. Among the problems, the existence of lipid rafts¹²⁻¹⁵ is the one that remains not clarified due to the lack of direct evidences. In the thesis, we introduced a super-resolution method (see Chapter 3 for the imaging results) that is able to image nanoscale phase separation of lipids that might provide a strategy to future development of lipid raft imaging field. The method involves the use of merocyanine 540 as a probe, and therefore it is possible that the monomer dimer equilibrium kinetics of MC540 participates behind the scene. Single molecule kinetic study using intensity time trajectory analysis (presented in Chapter 4) is used to evaluate potential kinetic schemes

involved. Below we give a brief introduction to the development and current status of the techniques that are involved.

Early history and development of single molecule spectroscopy and microscopy can be found in several reviews^{1, 6-9, 16-18}, here only recent progress in the field are highlighted.

Gene expression is one of many important essential life processes. Xie et al. showed¹⁹ how a immobilized fluorescent protein can be imaged in cells and applied to the task of watching real-time gene expression in live cells. A fusion protein of a yellow fluorescent protein (YFP) and a membrane targeting peptide was expressed under repressed condition. They showed that highly localized emitters (membrane-localized YFP) are able to give emission higher than autofluorescence background in *Escherichia coli* cells. Because the YFP they chose is a fast-maturing one, they were able to watch the gene expression in live cells, one molecule at a time. They, from the imaging results, noticed several qualitative features of the gene expression process: protein molecules (fusion protein) are generated in bursts, the number of protein molecules in each burst varies, and the bursts exhibit particular temporal spreads. They further gathered quantitative answers. The bursts (indicating the production of fusion protein) come in around 46 minutes in average. Each gene expression burst results from one mRNA molecule. On average, 4.2 protein molecules were produced from each mRNA. The posttranslational assembly of the fluorescent fusion protein was measured to be around 7 minutes.

Cohen and Moerner demonstrated²⁰ how a single biomolecule (fluorescently labeled tobacco mosaic virus) can be trapped by an anti-Brownian electrokinetic (ABEL) trap. This approach enabled extended period for the observation of single molecules in solution by applying counter electrokinetic forces to suppress Brownian motion of individual protein molecules in free solution, under ambient conditions. The Brownian motion of the biomolecule in the trap was monitored and a feedback voltage to a microfluidic cell was applied. The resulting electrokinetic forces produce a drift that cancels the Brownian motion exactly. Moerner et al further²¹ applied the trapping method to study the conformational dynamics of single β_2 -adrenergic receptors (β_2 ARs) in the solution phase. The activation process of the receptors is not a simple on-off switch. It is suggested a complex conformational landscape where multiple conformations with similar downstream activity are included in the active, signaling state. By gathering the fluorescence intensity and the excited-state lifetime for each single fluorescently labeled β_2 AR, the analysis showed that a complex conformational landscape is evidenced by a diversity of discrete values for fluorescence intensity and lifetime. The transitions among a range of intensity-lifetime states are observed. The intensity may be correlated, uncorrelated, or anticorrelated with lifetime. The time scale of the inter-conversion of these states is around hundreds of milliseconds, which indicates in the local protein environment.

Conformational dynamics of proteins may be viewed as itinerant motions when the protein traverses from one state to another on a complex network in conformational space (state space). Yang et al showed their method²² to extract the multiscale network in

state space from a single-molecule time series. The advantage of this approach is that the rules about the underlying dynamics about the system are objectively provided directly from the experimental single molecule time series without introduction of models that are postulated for the underlying physical mechanism.

Xie et al developed²³ a new method that is called “Ground-State Depletion Microscopy” that has ultrasensitive detection ability for optical absorption with single molecule sensitivity. Conducting single molecule level detection via fluorescent emission is known to be easier than via optical absorption due to the difference in the background interference (background free for emission method). The relative light attenuation for a single-molecule absorption process is no more than 10^{-6} - 10^{-7} , which is easily buried in the laser intensity noise (~1%), let alone the interference from Rayleigh scattering from sample inhomogeneity. Using a high-frequency dual-beam modulation transfer detection scheme to achieve ground state depletion in a pump probe setting, they were able to detect a single-molecule (Atto647N, Sigma-Aldrich, 04507) absorption signal at room temperature.

It can be seen that as the evolving development of single molecule spectroscopy and imaging methods keeps coming, new information regarding a biological system or process can be gathered to answer more fundamental questions in a microscopic approach. Watching gene expression process¹⁹, probing protein conformational dynamics landscape mapping^{20, 21}, and detecting optical absorption at single molecule level²³ are just a few of new methods that physical science researchers have been developing recently. On the

imaging front, one breakthrough is to be able to optically image biological sample with resolution that can succeed diffraction limit^{10, 24-26}.

Diffraction of light limits the ability of fluorescent microscopy to see the tiny details of an object under observation. It blurs the fine structures in the diffraction limited spot. By the Rayleigh Criterion, the resolution of a microscope is

$$R_0=0.61\lambda/NA$$

where λ is the wavelength of the emission light (detection) and NA is the numerical aperture of the objective lens. Two objects that are less than R_0 apart are impossible to distinguish if they emit at the same time. Therefore, structural details below 300 nm are usually missing when fluorescent microscopy are applied for the visualization. Lots of important biological process, usually involving interaction of proteins, falls in such spatial regime and therefore to remove such imaging barrier set by diffraction has been an active area^{25, 27-29} in scientific community. Among these methods, super-resolution microscopy²⁵ by single molecule localization has become a popular one for imaging nanostructure in cells.

The feasibility of super-resolution microscopy²⁵ by single molecule localization comes from two sources: sparse distribution of single molecule fluorescent emitters in each frame and high precision localization fitting of diffraction limited spots from these emitters. As long as these two requirements are guaranteed, repeated cycles of coordination collection from lots of frames enable the synthesis of a super-resolution image.

The high precision localization of fluorescent spots originates from the field of particle tracking³⁰. Single particles are imaged over time and are localized in every image. Particle trajectories can be created with position accuracy higher down to ~ 1 nm range³⁰. A two dimensional Gaussian function³¹ can be used to extract the centroid position of the spot and therefore the precise location of the emitter is read out. The localization of a diffraction limited spot from single molecule emitter gives the precise location of the emitter and is highly related to the number of photons that form the spot. Quantitatively, the localization precision³¹ can be estimated by:

$$\langle(\Delta x)^2\rangle = (s^2 + a^2/12)/N + 8 \pi s^4 b^2 / a^2 N^2$$

where $\langle(\Delta x)^2\rangle$ is the precision with which the fluorescent emitter can be localized in two dimensions, s is the standard deviation of the point spread function, N is the total number of photons collected (of the spot), a is the size of an image pixel, and b is the background noise per pixel. Therefore, the higher number of photons collected for each spot, the smaller the point spread function of the spot, the lower the background noise, and the smaller each pixel would give better localization accuracy. On the other hand, the idea of gathering distribution of single molecule fluorescent emitters in each frame to synthesis the final image was demonstrated by Hochstrasser³² et al by superimposing a series of single molecule spots from each frame to visualize nanostructures.

Generally speaking, there are three ways to achieve controlled sparse distribution of single molecule fluorescent emitters on each frame: photoactivated localization microscopy¹⁰ (PALM), stochastic optical reconstruction microscopy³³ (STORM), and point accumulation in nanoscale topology²⁶ (PAINT). The difference between them lies

in the use of various probes (dyes) to achieve active control of sparse distribution of single molecule emitters in each frame.

The PALM method uses photoactivable or photoswitchable fluorescent proteins, external laser enable photoactivation, and photobleaching to achieve the control. PALM has been used to resolve individual adhesion complexes and the spatial relationship between them and cytoskeleton and the substrate in migrating cells³⁴, and the nanoscale dynamics of the adhesion complexes in live cells³⁵ by Betzig et al. Baumgart³⁶ et al used the PALM method to analyze the spatial association of signaling proteins and F-actin effects. They found that after initiation of signaling, the spatial segregating of kinase ZAP70 and SLP76 signaling microclusters at eh cell periphery increases and that such segregation takes place in parallel with the reduction of microcluster phosphorylation levels. Moerner³⁷ et al used ParA-eYFP (targeted ParA filaments) and ParB-mCherry (targeted chromosome) fluorescent protein with the PALM method to observe the chromosome separation process guided by a spindle-like apparatus (40 nm wide linear spindle of ParA filaments). The information is obscured by diffraction by conventional microscopy.

The STORM method uses the same approach of photoactivation, photobleaching, yet with photoswitchable organic cyanine dyes (cy3-cy5). STORM has been applied to image molecular complexes, cells, and tissues with ~20 nm lateral and ~50 nm axial resolutions with three-dimensional data acquisition and multicolor approach^{24, 38, 39}. Clathrin-coated pits and microtubules in a cell were imaged with their 3D super-resolution approach by adding a cylindrical lens into the imaging path to distort the shape

point spread function to get the axial position of single molecule emitters³⁸. Recently, individual actin filaments in cells were resolved and the three-dimensional ultrastructure of the actin cytoskeleton was revealed using a dual-objective scheme with astigmatism imaging by the same group⁴⁰.

The PAINT method²⁶ is conceptually different from the aforementioned subdiffraction methods in that it relies on the control of thermal reaction rates to enable the switching between bright and dark states. Therefore, many conventional fluorescent probes can be applied in PAINT and the type of image will depend on the control of the interaction between the probe and its immediate environment by variations of probe parameters. PALM and STORM have proven to be useful to image nanostructures in cells, yet they rely on photoactivated proteins or photoswitching dyes, respectively and render them technically challenging. In the thesis, we are going to demonstrate an example of how the understanding of a dye and its interaction with the surrounding (lipid environment in our case) (chapter 4) and the integration of it with the PAINT method can envisage the nanoscale imaging of phase separation of lipids (chapter 3).

The concept of lipid rafts^{12, 41} has stimulated numerous biophysical studies^{13-15, 42} either by direct visualization techniques or indirect inferences^{43, 44} from the tracking and analysis of diffusing probes. Direct visualization techniques include electron microscopy⁴⁵ imaging of extracted portions of cell membranes, atomic force microscopy (AFM)^{46, 47} of supported lipid bilayers with various compositions that might emulate lipid rafts, fluorescent probe microscopy to expose partitioning between different phases on membranes^{48, 49}, coherent anti-Stokes Raman microscopy⁵⁰ of specific lipid domains, X-

ray scattering¹⁹ Mills, Thalia T. 2008_}, and NanoSIMS^{51, 52}. However a clear visualization of lipid rafts, which may vary in size from tens to several hundred nanometers on live cells, has not yet emerged. The ability to section cells along the axial directions and have sufficient lateral resolution to analyze raft domains remains a technical challenge. Therefore the development of methods that can readily distinguish lipid structures at high spatial resolution is essential. In this thesis, the “points accumulation for imaging in nanoscale topography” (PAINT) method²⁶, which has sub-diffraction resolution, is combined with a lipid phase-sensitive probe⁵³⁻⁵⁷, merocyanine 540 (MC540), to facilitate direct observation of phase separations on a supported lipid bilayer (to be detailed in the chapter 3), with the expectation that in the future the method might become applicable to cell membranes.

It is possible that the monomer dimer equilibrium is the underlying kinetics responsible for the blinking of the single molecule emitters in MC540 bound lipids based on previous researchers’ results^{55, 56, 58}. In the thesis, we are going to utilize the single molecule approach for the evaluation of possible kinetic scheme: analyzing the single molecule fluorescent intermittency (intensity time trajectory) (to be detailed in the chapter 4).

Single molecule intensity trajectory collection⁵⁹⁻⁶³ has been a powerful tool to see beyond the ensemble averaging, and therefore enable access to detailed information in various ways: (1) a probability density distribution function for an experimental observable, instead of a single, mean value, is provided; (2) static and dynamic heterogeneity of the observables can be differentiated; (3) statistically rare events, like

transitions between different functional states, can be explored; and (4) potential kinetic scheme can be evaluated through analysis of these distribution functions. The intermittency (on and off trajectory) of single molecule fluorescence time trace is caused, commonly, by the intensity to fluctuate among different levels, remain constant for irregular periods, and then fluctuate again. For a two-state system, the transitions occurred between high and low intensity levels and on time scale faster than the experimental time resolution. The bright state and dim state are referred to a so called on and off state, respectively. Methods⁶³⁻⁶⁶ have been employed to identify an intensity threshold that separates the on and off states, like a certain number of standard deviations above the average background signal or the local minimum between the on and off intensity peaks of the system's intensity histogram. Below several research examples are given regarding this approach. They show that single molecule intensity time trajectory can be very useful to study the fluctuation of the system (dynamic disorder), the heterogeneity of the system, and the interaction between molecules and their immediate environments.

Xie et al. re-examined^{59, 61, 67, 68} conventional Michaelis-Menton mechanism for a reaction catalyzed by an enzyme. They followed the enzymatic turnovers of single cholesterol oxidase molecules in real time by monitoring the emission from the enzyme's fluorescent active site, flavin adenine dinucleotide (FAD)⁵⁹. The fluctuation of the rate of cholesterol oxidation was revealed after detailed statistical analysis of the turnover and waiting time of the reaction. The dynamic disorder is shown by observing the apparent fluctuation of the catalytic rates due to the interconversion among different conformers of

the enzyme, having various catalytic rate constants. With the understanding that the real-time single molecule approach is able to extract the static disorder and dynamic disorder of reaction rates that were obscured in ensemble-average experiments, they further formulated the analysis^{60, 67-69} of the kinetic scheme with sequential intermediates. Based on the probability distribution function of on and off states, they derived a single-molecule Michaelis-Menten equation and found a linkage between the conventional macroscopic Michaelis-Menten model and the microscopic single molecule equations.

Recently, Peng et al. applied⁷⁰⁻⁷² a similar analysis on the kinetics of redox catalysis by single metal nanoparticles. Nanocrystals are important catalysts for many chemical transformations and are known to be heterogeneous due to their structural dispersions, and heterogeneous distribution of surface sites and surface restructuring dynamics. Using a single nanoparticle single turnover approach, they studied the redox catalysis of individual gold nanoparticles in solution by single molecule detection of fluorogenic reactions⁷⁰. They formulated the single molecule kinetic model of a Langmuir-Hinshelwood mechanism for heterogeneous catalysis by single nanocrystals^{71, 72}. They also extended the approach to study size effect on the catalytic activity of gold nanoparticles⁷³, and electrocatalysis activity by single-walled carbon nanotubes⁷⁴ and demonstrated the power of single-molecule approach in probing the heterogeneous and intricate workings of nanoscale catalysts.

Grondelle et al. developed a new statistical analysis technique⁷⁵ to extract reliable information, contained in large, discrete, and abrupt changes in the fluorescence signal level, which was easily obscured by the shot noise. The changes, if they are shorter than

the binning time used in the collection of a time trace, contain hidden dynamical information after averaging out by the binning process. They proposed a new approach to resolve similar shifts between discrete intensity levels by using primarily multiples of the standard deviation of the intensities. They performed single molecule level time trace collections on isolated pigment protein light harvesting complex of plants (LHCII) and utilized an algorithm that assigns a signal intensity change in a time trace to a large number of levels, rather than a simple two or three states. After the assigning, the intensity time trajectory is reconstructed according to the discrete levels sorted by the algorithm to remove the interference from shot noise. They showed that the popular two-state approach may not be a reasonable one for a system that contains multiple chromophores like LHCII. They further studied how the environment change⁷⁶ (acidity of the aqueous environment) accompanies the alteration of frequency of interchange between discrete states in LHCII. The efficiency of light harvesting (the probability for LHCII being in an on state) was found to be strongly affected by the local environment. In particular⁷⁶, as an acidic environment or a large incident photon flux is present, the efficiency of the light harvesting was greatly reduced.

A kinetic scheme of monomer dimer equilibrium (Scheme 3.1) of MC540 was proposed by Webb et al⁵⁸. It involves the interchange of two forms of MC540 monomers, one parallel to the lipids, and the other one perpendicular, and only the parallel form is directly linked to the formation and decomposition of dimers. It is likely that such kinetic scheme is responsible for what takes place in our super-resolution microscopy of lipid phases by using MC540 as a probe (see chapter 3). However, a more detailed analysis of

the single molecule intensity time trajectory of MC540 bound vesicles (see chapter 4) is performed to elucidate the possible kinetic schemes involved in our observation.

References for Chapter 1:

- (1) Moerner, W. E.; Fromm, D. P. Methods of Single-Molecule Fluorescence Spectroscopy and Microscopy. *Rev. Sci. Instrum.* **2003**, *74*, 3597-3619.
- (2) Moerner, W. E.; Kador, L. Finding a Single Molecule in a Haystack. Optical Detection and Spectroscopy of Single Absorbers in Solids. *Anal. Chem.* **1989**, *61*, 1217A-1223A.
- (3) Trautman, J. K.; Macklin, J. J.; Brus, L. E.; Betzig, E. Near-Field Spectroscopy of Single Molecules at Room Temperature. *Nature* **1994**, *369*, 40-42.
- (4) Betzig, E.; Chichester, R. J. Single Molecules Observed by Near-Field Scanning Optical Microscopy. *Science* **1993**, *262*, 1422-1425.
- (5) Xie, X. S.; Dunn, R. C. Probing Single Molecule Dynamics. *Science* **1994**, *265*, 361-364.
- (6) Lord, S. J.; Lee, H. D.; Moerner, W. E. Single-Molecule Spectroscopy and Imaging of Biomolecules in Living Cells. *Anal. Chem.* **2010**, *82*, 2192-2203.
- (7) Joo, C.; Balci, H.; Ishitsuka, Y.; Buranachai, C.; Ha, T. Advances in Single-Molecule Fluorescence Methods for Molecular Biology. *Annu. Rev. Biochem.* **2008**, *77*, 51-76.
- (8) Borgia, A.; Williams, P. M.; Clarke, J. Single-Molecule Studies of Protein Folding. *Annu. Rev. Biochem.* **2008**, *77*, 101-125.

- (9) Huang, B.; Bates, M.; Zhuang, X. Super-Resolution Fluorescence Microscopy. *Annu. Rev. Biochem.* **2009**, *78*, 993-1016.
- (10) Betzig, E.; Patterson, G. H.; Sougrat, R.; Lindwasser, O. W.; Olenych, S.; Bonifacino, J. S.; Davidson, M. W.; Lippincott-Schwartz, J.; Hess, H. F. Imaging Intracellular Fluorescent Proteins at Nanometer Resolution. *Science* **2006**, *313*, 1642-1645.
- (11) Bates, M.; Huang, B.; Dempsey, G. T.; Zhuang, X. Multicolor Super-Resolution Imaging with Photo-Switchable Fluorescent Probes. *Science* **2007**, *317*, 1749-1753.
- (12) Simons, K.; Ikonen, E. Functional Rafts in Cell Membranes. *Nature* **1997**, *387*, 569-572.
- (13) Munro, S. Lipid Rafts: Elusive Or Illusive? *Cell* **2003**, *115*, 377-388.
- (14) Cottingham, K. Do You Believe in Lipid Rafts? *Anal. Chem.* **2004**, *76*, 403 A-406 A.
- (15) Shaw, A. S. Lipid Rafts: Now You See them, Now You Don't. *Nat. Immunol.* **2006**, *7*, 1139-1142.
- (16) Livanec, P. W.; Dunn, R. C. Single-Molecule Probes of Lipid Membrane Structure. *Langmuir* **2008**, *24*, 14066-14073.
- (17) Zhuang, X. SINGLE-MOLECULE RNA SCIENCE. *Annu. Rev. Biophys. Biomol. Struct.* **2005**, *34*, 399-414.

- (18) Xie, X. S.; Trautman, J. K. OPTICAL STUDIES OF SINGLE MOLECULES AT ROOM TEMPERATURE. *Annu. Rev. Phys. Chem.* **1998**, *49*, 441-480.
- (19) Yu, J.; Xiao, J.; Ren, X.; Lao, K.; Xie, X. S. Probing Gene Expression in Live Cells, One Protein Molecule at a Time. *Science* **2006**, *311*, 1600-1603.
- (20) Cohen, A. E.; Moerner, W. E. Suppressing Brownian Motion of Individual Biomolecules in Solution. *Proceedings of the National Academy of Sciences of the United States of America* **2006**, *103*, 4362-4365.
- (21) Bockenhauer, S.; Färstenberg, A.; Yao, X. J.; Kobilka, B. K.; Moerner, W. E. Conformational Dynamics of Single G Protein-Coupled Receptors in Solution. *J Phys Chem B* **2011**, *115*, 13328-13338.
- (22) Li, C.; Yang, H.; Komatsuzaki, T. Multiscale Complex Network of Protein Conformational Fluctuations in Single-Molecule Time Series. *Proceedings of the National Academy of Sciences* **2008**, *105*, 536-541.
- (23) Chong, S.; Min, W.; Xie, X. S. Ground-State Depletion Microscopy: Detection Sensitivity of Single-Molecule Optical Absorption at Room Temperature. *J. Phys. Chem. Lett.* **2010**, *1*, 3316-3322.
- (24) Bates, M.; Huang, B.; Dempsey, G. T.; Zhuang, X. Multicolor Super-Resolution Imaging with Photo-Switchable Fluorescent Probes. *Science; Science* **2007**, *317*, 1749-1753.

- (25) Patterson, G.; Davidson, M.; Manley, S.; Lippincott-Schwartz, J. Superresolution Imaging using Single-Molecule Localization. *Annu. Rev. Phys. Chem.* **2010**, *61*, 345-367.
- (26) Sharonov, A.; Hochstrasser, R. M. Wide-Field Subdiffraction Imaging by Accumulated Binding of Diffusing Probes. *Proceedings of the National Academy of Sciences* **2006**, *103*, 18911-18916.
- (27) Hell, S. W.; Wichmann, J. Breaking the Diffraction Resolution Limit by Stimulated Emission: Stimulated-Emission-Depletion Fluorescence Microscopy. *Opt. Lett.* **1994**, *19*, 780-782.
- (28) Westphal, V.; Hell, S. W. Nanoscale Resolution in the Focal Plane of an Optical Microscope. *Phys. Rev. Lett.* **2005**, *94*, 143903.
- (29) Willig, K. I.; Rizzoli, S. O.; Westphal, V.; Jahn, R.; Hell, S. W. STED Microscopy Reveals that Synaptotagmin Remains Clustered After Synaptic Vesicle Exocytosis. *Nature* **2006**, *440*, 935-939.
- (30) Kural, C.; Kim, H.; Syed, S.; Goshima, G.; Gelfand, V. I.; Selvin, P. R. Kinesin and Dynein Move a Peroxisome in Vivo: A Tug-of-War Or Coordinated Movement? *Science* **2005**, *308*, 1469-1472.
- (31) Thompson, R. E.; Larson, D. R.; Webb, W. W. Precise Nanometer Localization Analysis for Individual Fluorescent Probes. *Biophys. J.* **2002**, *82*, 2775-2783.

- (32) Mei, E.; Sharonov, A.; Ferris, J. H.; Hochstrasser, R. M. Direct Visualization of Nanopatterns by Single-Molecule Imaging. *Appl. Phys. Lett.* **2005**, *86*, 043102.
- (33) Rust, M. J.; Bates, M.; Zhuang, X. Sub-Diffraction-Limit Imaging by Stochastic Optical Reconstruction Microscopy (STORM). *Nat Meth* **2006**, *3*, 793-796.
- (34) Shroff, H.; Galbraith, C. G.; Galbraith, J. A.; White, H.; Gillette, J.; Olenych, S.; Davidson, M. W.; Betzig, E. Dual-Color Superresolution Imaging of Genetically Expressed Probes within Individual Adhesion Complexes. *Proceedings of the National Academy of Sciences* **2007**, *104*, 20308-20313.
- (35) Shroff, H.; Galbraith, C. G.; Galbraith, J. A.; Betzig, E. Live-Cell Photoactivated Localization Microscopy of Nanoscale Adhesion Dynamics. *Nat Meth* **2008**, *5*, 417-423.
- (36) Hsu, C.; Baumgart, T. Spatial Association of Signaling Proteins and F-Actin Effects on Cluster Assembly Analyzed Via Photoactivation Localization Microscopy in T Cells. *PLoS ONE* **2011**, *6*, e23586.
- (37) Ptacin, J. L.; Lee, S. F.; Garner, E. C.; Toro, E.; Eckart, M.; Comolli, L. R.; Moerner, W. E.; Shapiro, L. A Spindle-Like Apparatus Guides Bacterial Chromosome Segregation. *Nat. Cell Biol.* **2010**, *12*, 791-798.
- (38) Huang, B.; Wang, W.; Bates, M.; Zhuang, X. Three-Dimensional Super-Resolution Imaging by Stochastic Optical Reconstruction Microscopy. *Science* **2008**, *319*, 810-813.

- (39) Huang, B.; Babcock, H.; Zhuang, X. Breaking the Diffraction Barrier: Super-Resolution Imaging of Cells. *Cell* **2010**, *143*, 1047-1058.
- (40) Xu, K.; Babcock, H. P.; Zhuang, X. Dual-Objective STORM Reveals Three-Dimensional Filament Organization in the Actin Cytoskeleton. *Nat Meth* **2012**, *advance online publication*.
- (41) Brown, D. A.; London, E. Structure and Origin of Ordered Lipid Domains in Biological Membranes. *J. Membr. Biol.* **1998**, *164*, 103-114.
- (42) Jacobson, K.; Mouritsen, O. G.; Anderson, R. G. W. Lipid Rafts: At a Crossroad between Cell Biology and Physics. *Nat. Cell Biol.* **2007**, *9*, 7-14.
- (43) Burns, A. R. Domain Structure in Model Membrane Bilayers Investigated by Simultaneous Atomic Force Microscopy and Fluorescence Imaging. *Langmuir* **2003**, *19*, 8358-8363.
- (44) Burns, A. R.; Frankel, D. J.; Buranda, T. Local Mobility in Lipid Domains of Supported Bilayers Characterized by Atomic Force Microscopy and Fluorescence Correlation Spectroscopy. **2005**, *89*, 1081-1093.
- (45) Magee, A.; Parmryd, I. Detergent-Resistant Membranes and the Protein Composition of Lipid Rafts. *Genome Biol.* **2003**, *4*, 234.

- (46) Yuan, C.; Furlong, J.; Burgos, P.; Johnston, L. J. The Size of Lipid Rafts: An Atomic Force Microscopy Study of Ganglioside GM1 Domains in Sphingomyelin/DOPC/Cholesterol Membranes. *2002*, *82*, 2526-2535.
- (47) Johnston, L. J. Nanoscale Imaging of Domains in Supported Lipid Membranes. *Langmuir* **2007**, *23*, 5886-5895.
- (48) Baumgart, T.; Hunt, G.; Farkas, E. R.; Webb, W. W.; Feigenson, G. W. Fluorescence Probe Partitioning between Lo/Ld Phases in Lipid Membranes. *Biochimica et Biophysica Acta (BBA) - Biomembranes* **2007**, *1768*, 2182-2194.
- (49) Heberle, F. A.; Buboltz, J. T.; Stringer, D.; Feigenson, G. W. Fluorescence Methods to Detect Phase Boundaries in Lipid Bilayer Mixtures. *Biochimica et Biophysica Acta (BBA) - Molecular Cell Research* **2005**, *1746*, 186-192.
- (50) Eric O. Potma, X. Sunney Xie Direct Visualization of Lipid Phase Segregation in Single Lipid Bilayers with Coherent Anti-Stokes Raman Scattering Microscopy. *ChemPhysChem* **2004**, *6*, 77-79.
- (51) Boxer, S. G.; Kraft, M. L.; Weber, P. K. Advances in Imaging Secondary Ion Mass Spectrometry for Biological Samples. *Annual Review of Biophysics* **2009**, *38*.
- (52) Kraft, M. L.; Weber, P. K.; Longo, M. L.; Hutcheon, I. D.; Boxer, S. G. Phase Separation of Lipid Membranes Analyzed with High-Resolution Secondary Ion Mass Spectrometry. *Science* **2006**, *313*, 1948-1951.

- (53) Yu, H.; Hui, S. Merocyanine 540 as a Probe to Monitor the Molecular Packing of Phosphatidylcholine: A Monolayer Epifluorescence Microscopy and Spectroscopy Study. *Biochimica et Biophysica Acta (BBA) - Biomembranes* **1992**, *1107*, 245-254.
- (54) Williamson, P.; Mattocks, K.; Schlegel, R. A. Merocyanine 540, a Fluorescent Probe Sensitive to Lipid Packing. *Biochim Biophys Acta*. **1983**, *732*, 387-393.
- (55) Verkman, A. S. Mechanism and Kinetics of Merocyanine 540 Binding to Phospholipid Membranes. *Biochemistry (N. Y.)* **1987**, *26*, 4050-4056.
- (56) Verkman, A. S.; Frosch, M. P. Temperature-Jump Studies of Merocyanine 540 Relaxation Kinetics in Lipid Bilayer Membranes. *Biochemistry (N. Y.)* **1985**, *24*, 7117-7122.
- (57) Ehrenberg, B.; Pevzner, E. Spectroscopic Properties of the Potentiometric Probe Merocyanine-540 in Solutions and in Liposomes. *Photochem. Photobiol.* **1993**, *57*, 228-234.
- (58) Dragsten, P. R.; Webb, W. W. Mechanism of the Membrane Potential Sensitivity of the Fluorescent Membrane Probe Merocyanine 540. *Biochemistry (N. Y.)* **1978**, *17*, 5228-5240.
- (59) Lu, H. P.; Xun, L.; Xie, X. S. Single-Molecule Enzymatic Dynamics. *Science* **1998**, *282*, 1877-1882.

- (60) Xie, X. S. Single-Molecule Approach to Dispersed Kinetics and Dynamic Disorder: Probing Conformational Fluctuation and Enzymatic Dynamics. *J. Chem. Phys.* **2002**, *117*, 11024-11032.
- (61) English, B. P.; Min, W.; van Oijen, A.,M.; Lee, K. T.; Luo, G.; Sun, H.; Cherayil, B. J.; Kou, S. C.; Xie, X. S. Ever-Fluctuating Single Enzyme Molecules: Michaelis-Menten Equation Revisited. *Nat Chem Biol* **2006**, *2*, 87-94.
- (62) Barbara, P. F.; Gesquiere, A. J.; Park, S.; Lee, Y. J. Single-Molecule Spectroscopy of Conjugated Polymers. *Acc. Chem. Res.* **2005**, *38*, 602-610.
- (63) Haase, M.; Hübner, C. G.; Reuther, E.; Herrmann, A.; Müllen, K.; Basché, T. Exponential and Power-Law Kinetics in Single-Molecule Fluorescence Intermittency. *J Phys Chem B* **2004**, *108*, 10445-10450.
- (64) Kuno, M.; Fromm, D. P.; Hamann, H. F.; Gallagher, A.; Nesbitt, D. J. "On"/"off" Fluorescence Intermittency of Single Semiconductor Quantum Dots. *J. Chem. Phys.* **2001**, *115*, 1028-1040.
- (65) Verberk, R.; Chon, J. W. M.; Gu, M.; Orrit, M. Environment-Dependent Blinking of Single Semiconductor Nanocrystals and Statistical Aging of Ensembles. *Physica E: Low-dimensional Systems and Nanostructures* **2005**, *26*, 19-23.
- (66) Naaman, O.; Aumentado, J. Poisson Transition Rates from Time-Domain Measurements with a Finite Bandwidth. *Phys. Rev. Lett.* **2006**, *96*, 100201.

- (67) Kou, S. C.; Cherayil, B. J.; Min, W.; English, B. P.; Xie, X. S. Single-Molecule Michaelis-Menten Equations. *J Phys Chem B* **2005**, *109*, 19068-19081.
- (68) Xie, S. Single-Molecule Approach to Enzymology. *Single Molecules* **2001**, *2*, 229-236.
- (69) Min, W.; English, B. P.; Luo, G.; Cherayil, B. J.; Kou, S. C.; Xie, X. S. Fluctuating Enzymes: Lessons from Single-Molecule Studies. *Acc. Chem. Res.* **2005**, *38*, 923-931.
- (70) Xu, W.; Kong, J. S.; Yeh, Y. E.; Chen, P. Single-Molecule Nanocatalysis Reveals Heterogeneous Reaction Pathways and Catalytic Dynamics. *Nat Mater* **2008**, *7*, 992-996.
- (71) Xu, W.; Kong, J. S.; Chen, P. Single-Molecule Kinetic Theory of Heterogeneous and Enzyme Catalysis. *J. Phys. Chem. C* **2009**, *113*, 2393-2404.
- (72) Chen, P.; Zhou, X.; Shen, H.; Andoy, N. M.; Choudhary, E.; Han, K.; Liu, G.; Meng, W. Single-Molecule Fluorescence Imaging of Nanocatalytic Processes. *Chem. Soc. Rev.* **2010**, *39*, 4560-4570.
- (73) Zhou, X.; Xu, W.; Liu, G.; Panda, D.; Chen, P. Size-Dependent Catalytic Activity and Dynamics of Gold Nanoparticles at the Single-Molecule Level. *J. Am. Chem. Soc.* **2010**, *132*, 138-146.

- (74) Xu, W.; Shen, H.; Kim, Y. J.; Zhou, X.; Liu, G.; Park, J.; Chen, P. Single-Molecule Electrocatalysis by Single-Walled Carbon Nanotubes. *Nano Lett.* **2009**, *9*, 3968-3973.
- (75) Krulger, T. P. J.; Iliescu, C.; van Grondelle, R. Fluorescence Intermittency from the Main Plant Light-Harvesting Complex: Resolving Shifts between Intensity Levels. *J Phys Chem B* **2011**, *115*, 5071-5082.
- (76) Krulger, T. P. J.; Iliescu, C.; Valkunas, L.; van Grondelle, R. Fluorescence Intermittency from the Main Plant Light-Harvesting Complex: Sensitivity to the Local Environment. *J Phys Chem B* **2011**, *115*, 5083-5095.

Chapter 2 Experimental Overview

2.1 Laser System

The continuous wave (CW) laser source used in the thesis includes a Kr^+ ion laser (National Laser Inc.) for 568 nm and a He-Ne solid state laser (Melles Griot, Carlsbad, CA) for 543.5 nm. If no other specification is made, the output horizontally or vertically polarized laser beam is made circularly polarized for both excitation wavelengths by quarter-wave plates. Appropriate excitation filters are used for both lasers.

2.2 Single Molecule Intensity-Time Trajectory and Spectra Measurement

2.2.1 Single Molecule Confocal Microscopy

2.2.1.1 Principle

The key to conducting spectral measurement or optical microscopy at single molecule level is the need to optimize signal to noise ratio¹. The principle of confocal microscope is briefly given here. In confocal microscopy, a pinhole is added to the image plane of the objective to enable small excitation volume and removal of out-of-focus signal to get high signal to noise ratio. The diameter of the pinhole determines the absolute depth of field for a confocal image. The term “confocal” refers to that the objective lens is used both for the illumination and the imaging of the sample. The collimated laser beam is focused to a diffraction-limited spot at the sample plane. The depth

resolution of a confocal microscope is approximately $d_z(3dB)=0.45\lambda/n(1-\cos\theta_0)$, where λ is the laser wavelength, n is the refractive index of the medium between the lens and the focal point, θ_0 and is the half angle subtended by the lens at its focus. The transverse resolution of a confocal microscope by the Sparrow criterion¹ is $d_{xy}=0.51/NA$, where NA is the numerical aperture and is given by $NA=n\sin\theta_0$. A high NA objective lens (~ 1.3) is usually used for single molecule detection. For $\lambda=543.5$ nm a NA=1.3 (oil) objective will give $d_{xy}=213$ nm. Raster scanning the sample stage underneath the laser spot is needed to form image of the sample. Therefore, the scanning stage requires high spatial precision and stability and is typically achieved by a computer-controlled piezo-electric stage.

2.2.1.2 The Setup

Scheme 2.1 shows the setup for the single molecule confocal microscope^{2,3} used in the thesis. The laser source as described above is used to provide continuous-wave excitation at 543.5 nm. The excitation beam (green line in the scheme) goes through appropriate excitation filters, is then directed by mirrors, passes through neutral density filters to adjust the incident powers (usually around 40 microwatts), and excites the sample through a high NA (~ 1.3) objective (Nikon FLUOR 40x) that is coupled with a piezo-electric stage (Queensgate) with closed-loop X-Y feedback for accurate sample positioning. The stage and objective is mounted Nikon Diaphot 300 microscope. The emission light passes through the same objective, goes through a pinhole, lens, notch filter to get rid of the residual excitation light, and appropriate emission filter sets before it is detected either by a sensitive Avalanche photodiode detector (APD) for imaging and

intensity trajectory or monochromator-attached charge coupled detector (CCD) camera for spectra recording.

The APD used in our setup has an active detection area of 170 nm by 170 nm. The high quantum efficiency of the APD (~70% around 500-700 nm) and high NA of the objective maximize the collection efficiency of the emitted photons to enable single molecule level detection. The dark counts of the APD detector is ~50 counts/s. The instrument response time of the detector is ~250 ps. The detector signal is then sent to a constant fraction discriminator (CFD). The CFD transforms the signal to transit-transit logic (TTL) pulses. A computer setup coupled with a controlled by Digital Instruments (DI) is then used to gather the signals for imaging purpose.

2.2.2 Intensity-Time Trajectory on Single Molecules

2.2.2.1 Principle

As long as a single molecule emitter has enough fluorescent quantum yield, confined spatially so it does not move transversely, and is photo-stable enough to endure long-time exposure to excitation, it may be coupled with high signal to noise ratio apparatus, such as confocal microscope with APD detector or TIRFM with wide field CCD camera to perform intensity-time trajectory collection. Binning of fluorescent signal to get the counts per unit time interval is usually required to get enough signal-to-noise ratio for display and analysis. As any other single molecule microscopy, the coverslips used in the experiment require excessive cleaning to give low to no background interference. The goal for such trajectory is to record the changes of fluorescent intensity

with time due to the conformational change of the emitting molecule, photochemical reaction associated with the change, or more complicated kinetics without the interference from photobleaching or diffusion of probes. One thing to remember is that the binning of fluorescent signal counts has to be properly adjusted so that it would blur the underlying kinetics involved for the formation of the intensity time trajectory. For example, if the presence of the on-state or off state happened on the time scale of microseconds or faster, such information will be easily lost in a trajectory that has millisecond time resolution. Usually a kinetic model is provided to get the solution for on-time an off-time probability function to compare with the experimental result. In chapter 4, such approach will be demonstrated as a way to verify what kind of kinetics happens in the intensity time trajectory in our studies.

2.2.2.2 The Setup

Traditionally, a TCSPC card with FIFO function attached to a computer has been a convenient way to collect intensity-time trajectory. In our lab, the TTL pulses from CFD (mentioned above in the microscope section) are sent to a NI board (National Instruments) with counter functions to achieve the binning of fluorescent counts against a external timing from a functional generator. Our home-made LabView program enables us to perform an image scan and localize on the fluorescent spot center for intensity time trajectory collection. The analysis of the on-time and off-time of each trajectory can also be performed on the go.

2.2.2.3 Data Processing and Analysis

Scheme 2.2 shows what an ideal intensity time trajectory looks like. One can easily notice that there are two signal levels³: one above (usually termed “on state”) the threshold level and one below (termed “off state”). The threshold level in our system is chosen to be always above the background level plus ten times of the shot noise from the signal to ensure no false identification is present in our analysis. Each length of the on-times and off-times is recorded separately and form a distribution function of on-times and off-times. The probability distribution function differs for different kinetics involved in the formation of the intensity time trajectory. Average on-time and off-time are calculated and exponential fits to the probability distribution function are provided to estimate the time scale and potential kinetics take place in the system. A home-made LabView, Mathematica, or Matlab program is used to perform such analysis and modeling.

2.2.3 Spectra Measurement

The fluorescence spectra were obtained on the microscope^{2, 3} where the fluorescence light is directed to a monochromator (Acton Research) equipped with a back-illumination liquid nitrogen cooled CCD camera (Princeton Instruments, Trenton, NJ).

2.3 Point Accumulation in Nanoscale Topology (PAINT)

2.3.1 Principle

In the PAINT method⁴, the object to be imaged is continuously targeted by fluorescent probes present in the system. The appearance of each fluorescent spot

depends on the interaction between the probe and the surroundings. Basically all single molecule fluorophores have their own intrinsic property to cause them to blink (switch on and off continuously). It may come from inherent photophysics, photochemical reactions, or conformational dynamics. As long as in each frame, only fluorescent images of the single molecules (well separated from each other by at least a distance close to diffraction limit) used as probe are recorded as diffraction limited spots. These spots can be subject to further 2D Gaussian fitting to extract their centroid positions. It has been shown such localization can get a spatial resolution close to 1 nm precision. These coordinates, which shows where these molecular interaction occur in high spatial resolution, are then gathered together from more than thousands of frames of images to display (synthesize) the spatial distribution image of these fluorophores. Therefore, lots of conventional dyes can be applied for nanoscale imaging as long as their interactions with specific surroundings and the formation of intensity time trajectory are understood. A tailoring of frame rates and experimental conditions can be made to record the blinking of single molecule fluorophores to form high resolution images that denote these interactions.

2.3.2 The Setup

The microscope^{2, 4} is based on a commercial Olympus (Melville, NY) IX81 inverted microscope and has been described previously. A circularly polarized Kr⁺ ion laser (568 nm) served as the excitation light source and was focused onto the back focal plane of an oil-immersion objective (Olympus 60 × NA = 1.45). Fluorescence from the sample was collected by the objective and directed to an EM-CCD camera (Roper Scientific, Tucson, AZ; Cascade 512F) by means of a dichroic mirror and an appropriate

set of band pass filters (Omega Optical Brattleboro, VT) to isolate the range 580 – 620 nm. A LabView (National Instruments) - based program was used to record sequences of images with various exposure times, frames, and collection rates. All measurements on the setup were conducted in TIRFM mode at ambient temperature (ca. 23 °C).

2.2.3 Data Processing and Analysis

The image analyzing procedures² for the PAINT method was described previously. Briefly, the first step is identification of the fluorescent spots frame-by-frame and the assignment of an approximate centroid coordinate to each spot. The latter assignment greatly reduced the computational search for the centroid. The coordinates were then refined by fitting each point spread function to two dimensional Gaussian functions:

$$I = A_0 + A \exp\left(-\frac{(x-x_0)^2}{2\sigma_x^2} - \frac{(y-y_0)^2}{2\sigma_y^2}\right)$$

, where $I(x,y)$ is an intensity signal, x_0 and y_0 are coordinates of the centroid, A_0 and A are the background level and signal amplitudes, and σ_x and σ_y are the widths of the point spread function. All computed spots were calibrated to stage drifting by coordinates of gold nanoparticle in each frame and then collected on one image frame to form the so-called synthetic image. The resolution was determined to be ca. 25 nm^{2,4} and therefore each spot was represented by a filled 25 nm diameter circle in the final synthetic image. In brief, only spots delivering more than 100 photons were accepted for analysis and the point spread function of our microscope has $\sigma=150$ nm. All the image gathering and analysis is done by a home-made LabView/Matlab program.

2.4 Polarization Dependent Measurements

2.4.1 Principle

Each molecule has its unique dipole moment and the orientation of dipole moment responsible for the emission and absorption can be probed by exciting a fluorophore with linearly polarized light. Only fluorophores with dipole moment that are in line with the direction of polarization of the incident light can pick up the excitation and show up in the corresponding fluorescent image.

2.4.2 The Setup

For wide-field epi-fluorescence polarization dependent imaging (section 4.3), our setup is the aforementioned commercial Olympus (Melville, NY) IX81 inverted microscope (section 2.3.2). Instead of operating under TIR mode, the linearly polarized beam (horizontally or vertically polarized after combinations of quarter waveplates and half waveplates) was sent in through the objective directly (standard mode) and epi-fluorescence is collected through the same objective. The image is captured by EM-CCD camera (Roper Scientific, Tucson, AZ; Cascade 512F) through a home-made LabView program.

For polarization dependent PAINT imaging (section 4.3), the setup is exactly the same as the one in 2.3.2 except the excitation beam is now either vertically or horizontally polarized sent in through TIR mode and gives p-polarized (X and Z direction in laboratory coordinates) or s-polarized (Y direction in laboratory coordinates) excitation evanescent wave.

2.4.3 Data Processing and Analysis

For wide-field epi-fluorescence, the image is used directly for further interpretation.

For polarization dependent PAINT imaging, the synthesized images (coordinates of spots) are selected in cross-section through either X- or Y- direction and divided them into ten bins spatially to perform histogram analysis. The number density distribution profile is then compared with the one from circularly polarized excitation to see how the spatial distribution of emitting dipole moments varies according to the preferential polarized excitation.

2.5 Materials and Experimental Conditions

2.5.1 Materials and Sample Preparations.

Materials

Merocyanine 540 (see scheme 2.3 for the molecular structure of MC540) was purchased from AnaSpect (San Jose, CA) and used without further purification. Lipids (DOPC, 1,2-Dioleoyl-sn-Glycero-3-phosphocholine, DLPC, 1,2-dilauroyl-sn-glycero-3-phosphocholine, DMPC, 1,2-Dimyristoyl-sn-Glycero-3-phosphocholine, and DPPC, 1,2-dipalmitoyl-sn-glycero-3-phosphocholine) were purchased from AvantiPolar Lipids (Alabaster, AL) and used as received. Nile red was purchased from Invitrogen (Carlsbad,

CA) and used as received. PBS buffer were from Fisher Scientific (Hampton, NH). Chloroform was from Acros Organics (Geel, Belgium).

Sample Preparatons

Supported lipid bilayers (SLB) by vesicle fusion method for formation.

The preparation of large unilamellar vesicles and supported lipid bilayers followed commonly used procedures⁵⁻⁸. Lipid or lipid mixtures that contain either DOPC, DPPC or 3:1 molar ratio mixture of DOPC over DPPC were dissolved in chloroform then dried under a nitrogen stream and pumped for more than two hours to remove residual chloroform. The lipids were re-suspended at 1mM in pH 7.4 PBS buffer and vortexed vigorously for 1 hour prior to five freeze-thaw circles. They were extruded 20 times through a 100 nm-pore polycarbonate membrane (Avanti Polar Lipids) at 60 °C for DPPC or DOPC/DPPC mixture, or 25 °C for DPPC. Here they formed large unilamellar vesicles (LUV) solutions. The vesicle (LUV) solutions were then deposited on coverslips held at 60 °C by a heated water bath. After 30 minutes, pH 7.4 PBS buffers pre-heated to 60 °C were added into the dishes to keep the samples from drying over 90 minutes of further heating. The samples were cooled to room temperature overnight by which time the supported lipid bilayers were formed on the coverslips. Extensive washing with pH 7.4 PBS buffer removed residual lipids. The samples on the coverslips were then stored in pH 7.4 PBS buffer.

Large unilamellar vesicles (LUV, ~100 nm in size) by the standard extrusion method.

The preparation of LUV was done by the following procedure³: 1 mM lipid solution in chloroform in a glass vial was blown by constant nitrogen flow to evaporate the solvent, leaving a dry phospholipid film on the internal surface of the vial. The vial was kept under vacuum for 2 hours before the lipid film was then hydrated in 1 mL of phosphate buffer (20 mM, pH 7.0) under continuous stirring at temperature above their critical temperature for 90 minutes. The resulting multilamellar vesicles were subject to five freeze/thaw cycles and extruded more than 20 times through 100 nm polycarbonate membranes (Whatman, Florham Park, NJ) through a MiniExtruder (Avanti Polar Lipids). Vesicles were used within 1 or 2 days of preparation.

Giant unilamellar vesicles (GUV) by the electroformation method.

The GUVs were prepared by electroformation⁹. 10 μ L of 0.2 mg/mL lipid solution in chloroform was deposited on indium tin oxide (ITO) coated glass and subsequently dried by a nitrogen flow and in vacuum for 1 h. The GUVs were grown in an electric field applied between two ITO coated glass plates separated by a 2 mm rubber spacer. A 10 Hz sinusoidal voltage was applied to the electrodes at 0.5 V/mm while the chamber was filled with 0.2 M sucrose solution. The electric field was gradually raised up to 1.5 V/mm in steps of 0.1 V, applied every 5 min by means of a function generator, based on an NI-DAC board (National Instruments). The growth of the vesicles was visually monitored by differential interference contrast (DIC) microscopy. Vesicle formation was

continued for 1 h at 1.5 V/mm. The GUVs were then gently removed by a syringe and stored at 4 °C.

Nanobead –supported Bilayers

The sample is a gift from Yong-ho Kim from Degrado's group. The preparation procedure can be found in their publication¹⁰.

2.5.2 Experimental Conditions

For imaging experiments, a cylinder was placed on top of the coverslip on the sample stage to confine the PBS solution (volume ~200 μ l). The PBS solution is sucked out before the addition of the probe solution. The probe solution was added to the sample holder until the surface number density of fluorescent spots was optimized at 0.75 μm^{-2} . Note here only the amounts of probe molecules are increased without change the solution concentration. Gold nanoparticles (50 nm) were added so that several of them were visible in the field of view: they served as standards to correct for mechanical drifting of the stage during the frame scan. Usually ~20K frames were recorded in 5 minutes.

For intensity-time trajectory collection, a cylinder was placed on top of the coverslip on the sample stage to confine the PBS solution (volume ~1 ml). The PBS solution is sucked out before the addition of the LUV solution. 30 minutes after the LUV solution was added, the solution was removed and washed several times with PBS solution to ensure the LUVs are well separated from each other on the glass surface. The

MC 540 stock solution was then added to the sample vial with either 200 μl , 300 μl , 400 μl , 500 μl , or 600 μl of total volume of the stock solution. Note that the stock solution used for different type of lipid differs so that the average off-time of the intensity-time trajectory was observed for further analysis.

Coverslip cleaning procedure

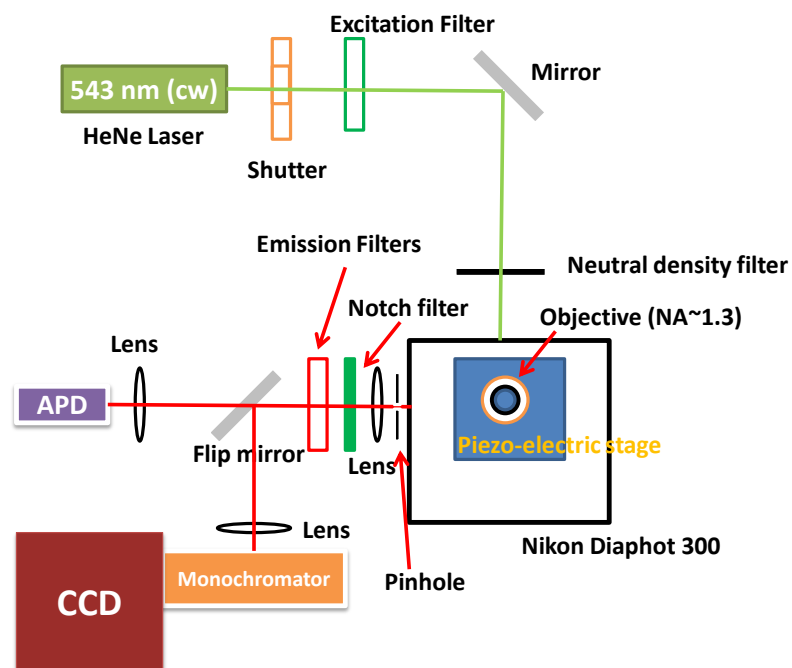
Glass coverslips (Fisher Scientific) and cylinders (Bioptechs, Butler, PA) were sonicated for over 1 hr in piranha solution (3:1 mixture of sulfuric acid and 30% hydrogen peroxide) and followed by extensive washing and rinsing by UltraPure water (Millipore, Billerica, MA) to suppress background fluorescence. A high voltage UV lamp is used to bleach organic contaminants by irradiating the cleaned coverslips for more than 30 minutes.

References for Chapter 2:

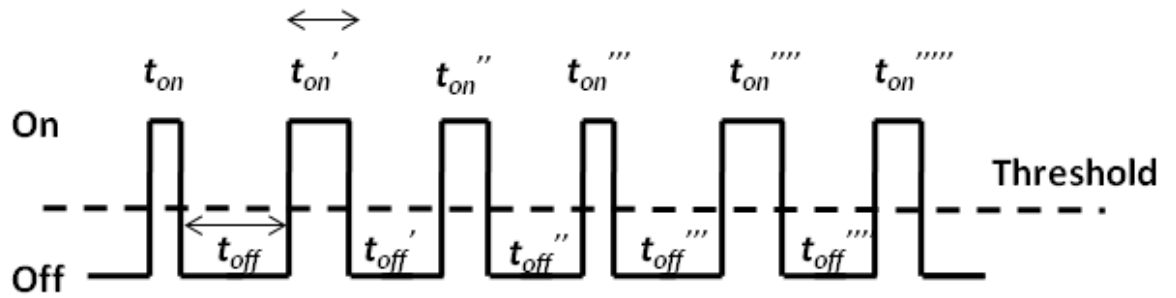
- (1) Moerner, W. E.; Fromm, D. P. Methods of Single-Molecule Fluorescence Spectroscopy and Microscopy. *Rev. Sci. Instrum.* **2003**, *74*, 3597-3619.
- (2) Kuo, C.; Hochstrasser, R. M. Super-Resolution Microscopy of Lipid Bilayer Phases. *J. Am. Chem. Soc.* **2011**, *133*, 4664-4667.
- (3) Gao, F.; Mei, E.; Lim, M.; Hochstrasser, R. M. Probing Lipid Vesicles by Bimolecular Association and Dissociation Trajectories of Single Molecules. *J. Am. Chem. Soc.* **2006**, *128*, 4814-4822.
- (4) Sharonov, A.; Hochstrasser, R. M. Wide-Field Subdiffraction Imaging by Accumulated Binding of Diffusing Probes. *Proceedings of the National Academy of Sciences* **2006**, *103*, 18911-18916.
- (5) Boxer, S. G.; Kraft, M. L.; Weber, P. K. Advances in Imaging Secondary Ion Mass Spectrometry for Biological Samples. *Annual Review of Biophysics* **2009**, *38*.
- (6) Burns, A. R. Domain Structure in Model Membrane Bilayers Investigated by Simultaneous Atomic Force Microscopy and Fluorescence Imaging. *Langmuir* **2003**, *19*, 8358-8363.
- (7) Burns, A. R.; Frankel, D. J.; Buranda, T. Local Mobility in Lipid Domains of Supported Bilayers Characterized by Atomic Force Microscopy and Fluorescence Correlation Spectroscopy. **2005**, *89*, 1081-1093.

- (8) Cremer, P. S.; Boxer, S. G. Formation and Spreading of Lipid Bilayers on Planar Glass Supports. *The Journal of Physical Chemistry B* **1999**, *103*, 2554-2559.
- (9) Angelova, M.; Dimitrov, D. In *A mechanism of liposome electroformation; Trends in Colloid and Interface Science II*; Degiorgio, V., Ed.; Springer Berlin / Heidelberg: 1988; Vol. 76, pp 59-67.
- (10) Kim, Y. H.; Donald, J. E.; Grigoryan, G.; Leser, G. P.; Fadeev, A. Y.; Lamb, R. A.; DeGrado, W. F. Capture and Imaging of a Prehairpin Fusion Intermediate of the Paramyxovirus PIV5. *Proceedings of the National Academy of Sciences* **2011**, *108*, 20992-20997.

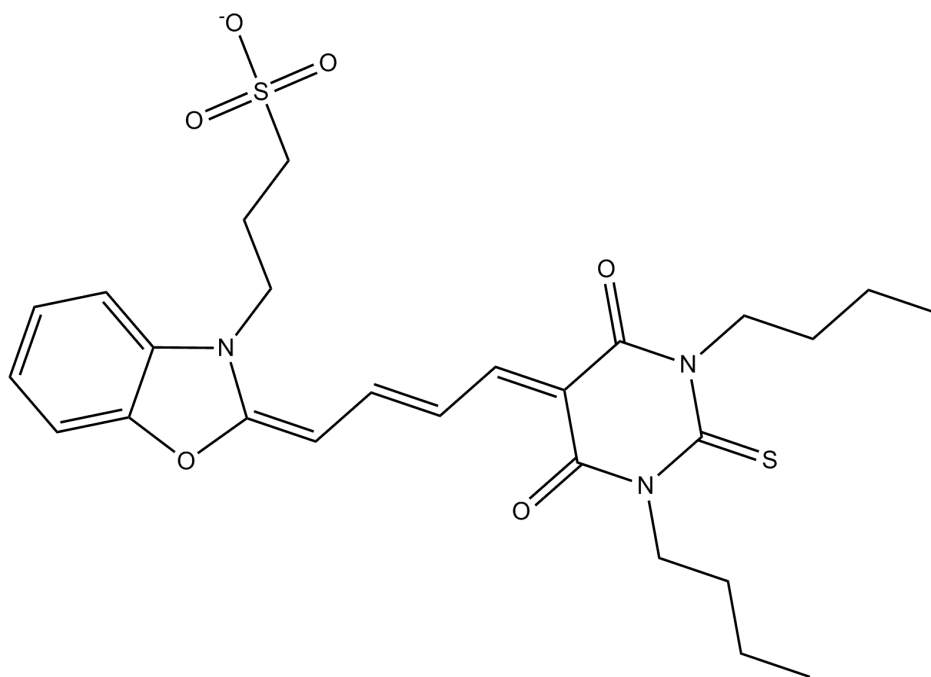
Schemes for Chapter 2:



Scheme 2.1. The experimental setup for the single molecule confocal microscopy used in our studies.



Scheme 2.2. An ideal intensity time trajectory. The dashed line denotes the threshold level to separate the signals into on or off states.



Scheme 2.3. Molecular Structure of Merocyanine 540

Chapter 3 Super-resolution Microscopy of Lipid Bilayer Phases

3.1 Introduction

The goal of visualizing the nanoscopic sphingolipid/cholesterol-rich domain¹⁻⁵ in natural membranes has stimulated numerous investigations either by direct visualization⁶⁻¹⁴ or indirect inferences^{7, 8, 15} from the tracking of diffusing probes. Direct methods include electron microscopy of cell membranes^{8, 13}, atomic force microscopy (AFM)^{7, 8, 16} of supported lipid bilayers, fluorescent probe microscopy^{8, 10, 11, 17, 18} of different phases, coherent anti-Stokes Raman microscopy⁹ of lipid domains, X-ray scattering¹⁴, and NanoSIMS^{6, 12}. Nevertheless visualization or systemization of such domains (rafts), assumed to vary from tens to several hundred nanometers¹⁶ in cell membranes^{1, 3, 4, 8}, remains challenging. In this chapter, the “points accumulation for imaging in nanoscale topography” (PAINT) method¹⁹, which has sub-diffraction resolution, is combined with a lipid phase-sensitive probe merocyanine 540 (MC540 hereafter), to illustrate that nanoscale phase separations on a supported lipid bilayer (SLB) can be visualized by this method.

The PAINT method of Sharonov and Hochstrasser¹⁹ is based on the accumulation of centroid coordinates of single molecule fluorescence images. The lateral resolution is ~25 nm¹⁹. The processing procedure is similar to that first introduced in the PALM²⁰ imaging method and subsequently in STORM²¹: the fluorophores are switched on or off between frames and the coordinates of a subset of fluorophores in each frame are

obtained. The point spread function of each molecule is then fitted to a two dimensional Gaussian to determine its peak coordinates. By accumulating coordinates from many frames, an image of points is constructed that represents the spatial distribution of fluorophores. The PAINt method¹⁹ is conceptually different from the aforementioned subdiffraction methods^{20,21} in that it relies on the control of thermal reaction rates to enable the switching between bright and dark states. Therefore, many conventional fluorescent probes can be applied in PAINt and the type of image will depend on the control of the interaction between the probe and its immediate environment by variations of probe parameters. The PALM and STORM methods use external laser switching of photoactivable probes in combination with photobleaching. One useful example of PAINt has used Nile Red¹⁹, which has a distinctive fluorescence signal when associated with micelles and lipid bilayers but is only weakly fluorescent in water. Therefore, it has been used to obtain sub-diffraction images of vesicles, and super-resolution contour maps of supported lipid bilayers¹⁹. The switching of the Nile Red between bright and dark states is dependent on its flux to into lipids and by photobleaching²³. However, the fluorescence of Nile Red has not proven to be sensitive to the phase of the lipid. Therefore we have sought other possible probes of that will provide PAINt images of lipid phase domains.

3.2 Properties of Merocyanine as a probe in lipids

Merocyanine 540 is sensitive to lipid structure²⁴⁻²⁷ and has voltage sensitivity^{28, 29}, so it has been widely employed as a probe particularly for the measurement of membrane

potentials³⁰. It has been applied in epifluorescence microscopy to image phase domains in supported lipid monolayers²⁶. Its absorption and fluorescence in aqueous and nonpolar lipid environments are distinctive³¹⁻³⁴. It emits very weakly in aqueous solution compared with lipid which makes possible single molecule experiments on lipid bound probes.

In aqueous solution containing lipid bilayers, MC 540 migrates to the hydrophobic regions^{28, 31, 32}. Above a certain [Lipid]/[MC 540] threshold^{31-33, 35, 36}, it mainly exists as monomers or dimers in the lipid. The dimer form is prevalent in most lipids but the equilibrium is sensitive to the lipid packing order. The apparent dimerization equilibrium constants (ratios of the dimer concentration to the square of the monomer concentration) in phosphatidylcholine (PC) suspensions are in the range of 10^3 to 10^6 M⁻¹, depending on the lipid packing, temperature, and [lipid]/[MC 540] ratio^{31, 32, 37, 38}. The kinetics leading to the attainment of the monomer-dimer equilibrium have been studied by several research groups^{28, 31, 32, 36, 39}. The presence of two forms²⁸ of the monomer is indicated: one with its approximate pi-electron plane parallel ($M_{//}$) and the other perpendicular (M_{\perp}) to the membrane surface. The dimer is oriented with its monomer planes parallel to the membrane surface. The kinetic parameters introduced in Scheme 3.1 are supported by several studies^{28, 31, 32, 39} and those for MC 540 in PC vesicles^{31, 32} are typical. The present experiments are conducted at concentrations suitable for isolation of single molecules of monomeric MC 540, where the ratio [lipid]/[MC 540] is very large. According to previous studies^{26, 27, 31, 35-38, 40}, the monomer-dimer equilibrium exhibits sensitivity to the lipid phase. These properties render MC 540 a potentially useful probe of membrane domain structure.

3.3 Spectra measurement results of MC540 in liposomes

The monomeric form of MC 540 in liposomes absorbs at 570 nm and emits at 590 nm^{24, 33, 36}. The fluorescence yield of monomeric MC540 is reported as 0.6 in DMPC liposomes and micelles while in water it is 0.05²⁷. Dimeric MC 540 in liposomes absorbs at 540 nm and emits with low yield at 625 nm^{25, 38}. In the present work, fluorescence spectra were recorded for DOPC SLB and DPPC SLB containing MC 540. The details for the materials, preparation of samples, and confocal microscopy setup used for the spectra measurement are given in the chapter 2. The emission spectra (Figure 3.1A and 3.1B) match those reported for monomeric MC 540. The concentration used in these fluorescence spectra measurements was 10 times higher than in the PAINT experiments and only monomer fluorescence was seen. The fluorescent intensity of MC 540 in DOPC SLB is ca. 8 times larger than that in DPPC SLB when the same amount of MC 540 is added as seen from Figure 3.1A. When an additional volume of the MC 540 stock solution is added systematically to the DPPC SLB sample, the fluorescent intensity increases (see Figure 3.1B). The same effect was found for the DOPC SLB sample (data not shown). The spectral shape is not concentration dependent within our signal to noise. The dimer emission is never identified because of its weakness. The spectra (Figure 3.1) are reported 10X the concentration used for the PAINT experiments in order to provide a reasonable signal-to-noise for display. These results suggested that the monomer-dimer equilibrium of MC 540 in the lipid phase is influencing the observed fluorescence

intensities. This conclusion is further supported by the intensity increases being proportional to the square root of the volume added (see Figure 3.1B and 3.1C).

The fluorescence decay of MC 540 in liposomes^{24, 36} has a 2 ns component, attributed to the perpendicular monomer, and a ca. 800 ps component from the parallel monomer. The amplitude ratio of the longer to the shorter lifetime component is greater than 6 in the liquid phase LUV and 1.5 for the gel phase¹⁴. Therefore, these photophysical parameters^{14, 24} and the kinetic measurements by Verkman et al.^{31, 32} support the conclusion that the major emitting species exhibiting stronger fluorescence in the liquid compared with the gel phase LUV is the perpendicular monomeric MC540.

3.4 Imaging results and discussions

For a given concentration, the number density of monomeric MC 540 should be higher in the liquid phase where K_d is around $4 \times 10^3 \text{ M}^{-1}$, than in the gel phase where K_d is approximately $1.7 \times 10^5 \text{ M}^{-1}$ ^{31, 32, 37}. It is evident from the absorbance peaks at 570 nm and at 540 nm that the gel phase LUV (large unilamellar vesicle) has a larger dimer/monomer ratio at equilibrium than the liquid phase LUV^{24, 33, 34}, although the dimer is the predominant form of lipid associated MC540 in both cases. On the bilayer (DOPC:DPPC=3:1) principally studied here, the liquid phase region is calculated to have a larger number density of monomeric MC 540 than the gel phase region (see Figure 3.2B). The monomer concentration equals the square root of the dimer concentration (which involves almost all of the added MC 540 molecules under the present conditions) divided by the equilibrium constant. Therefore, the integrated fluorescence intensity

(from Figure 3.1C, red curve) and the number density of bursts (from Figure 3.2A, red and green curves) should vary as the square root of the volume of MC 540 stock solution added, which determines the total number of MC 540 molecules in the sample. The influence of a monomer-dimer equilibrium of this type is evident from these observed fluorescence intensities.

The PAINT sub-diffraction microscopy utilizes the stochastic appearance of fluorescent bursts from single molecules. Given the parameters in Scheme 3.1, the species $M_{//}$ has mean existence time of ca. $3\ \mu\text{s}$ whereas M_{\wedge} survives for an average time of 3 ms. Both these periods are considerably shorter than the framing time of the present experiment which is 16 ms. Therefore a particular monomer signal does not show up in successive frames. The synthetic image shown in Figure 3A, is composed of the distribution of fitted points at which single molecules appear (visits). The image projects the spatial distribution of monomeric MC 540 on the DOPC/DPPC, 3:1 supported lipid membrane (The SLB preparation is described in the Chapter 2). Such images could be constructed in less than 90s by accumulating ca. 10^5 points from 7500 frames. Each point represents one visit of a monomeric MC 540. The total number of spots displayed in figure 3.3A is kept high enough to reveal domains whose sizes are larger than or close to the diffraction limit. As will be demonstrated below, the nano-domains become more clearly identified when more spots are accumulated. Nevertheless it is evident from the image in Figure 3.3A that there are both bright and dark spatial regions. Three regions having different number density of monomer appearances from Figure 3.3A can be defined. They are: the liquid phase region, which has the largest number of visits; the gel

phase region; and the coverslip region, which has the lowest number (see Figure 3.2A). In contrast, the accumulated TIRFM image at the diffraction limit is blurred (Figure 3.3B). The ratio of the number density of monomeric MC 540 in the liquid phase over that in the gel phase region is determined (Figure 3.2A) to be ca. 3, consistent with the prediction from the liposome dimerization constants data (Figure 3.2B).

Experimental results are discussed below where Nile Red and MC540 were used successively on the same lipid. The Nile Red was first used to obtain a PAINT image then the sample was repeatedly washed with PBS solution to remove all trace of Nile Red emission after which MC 540 was added. Gold nanoparticles were used to calibrate any drifts of the stage during this procedure. The lipid is expected to spread spontaneously over even rough or scratched parts of the glass surface if the regions are hydrated.⁴¹

Gel phase domains smaller than 100 nm were seen when ca. 50,000 frames were accumulated at a number density of ca. $0.6 \mu\text{m}^{-2}$. Rainbow colors are used in Figure 4 to emphasize that there are regions having fewer bright spots per unit area. In contrast, Nile Red microscopy carried out on the same spatial region, displayed a homogenous distribution of emitters (Figure 4A). When MC 540 is used as the probe, Figure 4B, the emission patterns are heterogenous with bright and dark regions being clearly seen. The darker regions are identified as gel phase domains of DOPC:DPPC 3:1 SLB. There are several nanoscopic domains present in the image. To the best of our knowledge, this is the first time that such nanoscopic domains have been observed using an optical microscope.

The phase diagram⁴² for the composition of DOPC:DPPC indicates that it is a mixture of gel and liquid phase for DOPC:DPPC=3:1 at ambient temperature. The morphology of supported lipid bilayers of DOPC:DPPC=3:1 on a glass coverslip was studied by means of AFM by Burns⁴³. It was confirmed that there is coexistence of liquid and gel phase⁴³, and that the dimension of the gel phase domains range from tens of nm to mm. The optical microscopy presented herein is entirely consistent with the AFM.

At the concentration of MC 540 in the lipid and the light intensity used, monomers would require to be localized for at least ca. 0.5 ms to form a single molecule image. Therefore the model envisaged has the monomers immobilized, perhaps by locking the charged SO₂⁻ group to the polar surface of the bilayer (The molecular structure of MC 540 is shown in the scheme 2.3). But the photon burst time must be short compared with the frame time of 16 ms because successive images are not spatially correlated, even at the lowest power. The monomer signals are assumed to appear as a result of dissociation of the nonfluorescent dimers. If lateral diffusion of localized monomers tracks the lipid diffusion of ca. 6 to 8.3 $\mu\text{m}^2\text{s}^{-1}$ the image would not be blurred if the burst time were ca. 2 ms or less. A reversible photo bleaching might contribute to this burst.

The kinetic processes underlying the PAINT signals were also evaluated by single molecule measurements in a confocal geometry. The single molecule spots show telegraph signal trajectories having a mean on-time of 3 ms independent of the concentrations (see the figure 4.3 from chapter 4). The much longer (10-100 ms) mean off-time is dependent both on the MC540 number density and on the type of lipid. These

results are consistent with but do not prove that the monomers are undergoing equilibrium kinetics of the type expected from Scheme 3.1. We confirmed that the number density of monomers in the gel phase is lower than in the liquid phase for the same total number density of MC 540 in accord with the conclusions drawn from the TIRFM measurements. This part of result and discussion will be detailed in chapter 4.

Conventional photophysical steps are too fast to account for the observed on and off trajectories. Fluorescence correlation²² of MC540 in ethanol showed that trans-cis isomerization and triplet state formation take place on the ms and ns and time scales respectively, both shorter than the ms frame time of the present experiments. Although the isomerization might be slowed down by the lipid it is unlikely to be concentration dependent as is the slow off-time measured in this work. Moreover, MC540 molecules may photobleach by forming non-fluorescent states that recover the ground state of the fluorescent MC540 on the ms time scale by pathways that depend on the coupling between probes. While it cannot be ruled out that the isomerization might be slowed down dramatically in the lipid or that other photoproducts are involved, the processes that contribute to the phase separation imaging would require to have a number of essential features, as discussed above: a ms relaxation time; an off-time that depends on the number density of MC540; and a variation of these properties with the lipid phase. The number density dependence ensures that the process is not a simple two state equilibration between a fluorescent and nonfluorescent state.

3.6 Conclusion

It was shown that the PAINT method of super-resolution imaging using the dye MC540 is useful for imaging nanoscale phase domains in binary lipid bilayers. The monomer-dimer dynamic equilibrium of MC 540 in lipids is essential to the repopulation of photobleached monomers. The distinction between lipid phases arises because the average number density of fluorescent monomeric MC 540 molecules in the liquid phase of the supported lipid bilayers is ca. 3 times larger than that in gel phase. The synthetic image (the PAINT image) was obtained by superimposing all fitted single molecule points and applying pseudo color mapping, thereby revealing phase separation of DOPC:DPPC 3:1 at subdiffraction resolution. Many nanoscopic domains of the gel phase were seen. The extension of this method to other binary or ternary lipid model or natural systems provides a promising new super-resolution strategy.

A variety of probes have previously been employed to image phase separation by optical microscopy¹⁸. They are now obvious candidates for PAINT microscopy. However, MC 540 is unique in that it does not appear to rely only on the population partitioning between phases but on the phase dependence of the monomer-dimer equilibrium. The lipids contain both monomeric and dimeric forms of MC 540 present in dynamic equilibrium and the large excess of dimer serves as the reservoir for the fluorescent, monomeric MC 540. Therefore, the single molecule fluorescent spots can be collected sparsely in each frame as required by this type of sub-diffraction optical microscopy.

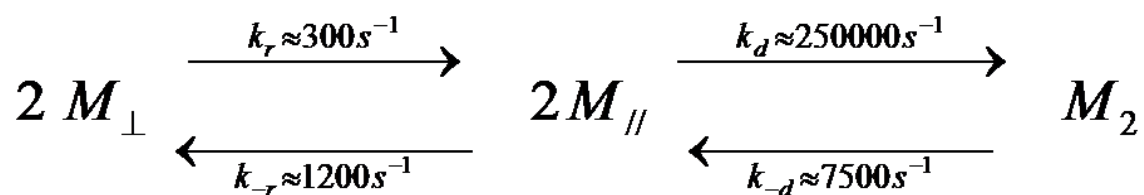
References for Chapter 3:

- (1) Cottingham, K. *Anal. Chem.* **2004**, 76, 403A.
- (2) Jacobson, K.; Mouritsen, O. G.; Anderson, R. G. W. *Nat. Cell Biol.* **2007**, 9, 7.
- (3) Munro, S. *Cell* **2003**, 115, 377.
- (4) Shaw, A. S. *Nat. Immunol.* **2006**, 7, 1139.
- (5) Simons, K.; Ikonen, E. *Nature* **1997**, 387, 569.
- (6) Boxer, S. G.; Kraft, M. L.; Weber, P. K. *Annu. Rev. Biophys.* **2009**, 38.
- (7) Burns, A. R.; Frankel, D. J.; Buranda, T. *Biophys. J.* **2005**, 89, 1081.
- (8) Elson, E. L.; Fried, E.; Dolbow, J. E.; Genin, G. M. *Annu. Rev. Biophys.* **2010**, 39, 207.
- (9) Potma, E. O.; Xie, X. S. *ChemPhysChem* **2004**, 6, 77.
- (10) Gaus, K.; Gratton, E.; Kable, E. P. W.; Jones, A. S.; Gelissen, I.; Kritharides, L.; Jessup, W. *Proc. Natl. Acad. Sci. U.S.A.* **2003**, 100, 15554.
- (11) Johnston, L. J. *Langmuir* **2007**, 23, 5886.
- (12) Kraft, M. L.; Weber, P. K.; Longo, M. L.; Hutcheon, I. D.; Boxer, S. G. *Science* **2006**, 313, 1948.
- (13) Magee, A.; Parmryd, I. *Genome Biol.* **2003**, 4, 234.
- (14) Mills, T. T.; Tristram-Nagle, S.; Heberle, F. A.; Morales, N. F.; Zhao, J.; Wu, J.; Toombes, G. E. S.; Nagle, J. F.; Feigenson, G. W. *Biophys. J.* **2008**, 95, 682.
- (15) Korlach, J.; Schwille, P.; Webb, W. W.; Feigenson, G. W. *Proc. Natl. Acad. Sci. U.S.A.* **1999**, 96, 8461.
- (16) Yuan, C.; Furlong, J.; Burgos, P.; Johnston, L. J. *Biophys. J.* **2002**, 82, 2526.

- (17) Heberle, F. A.; Buboltz, J. T.; Stringer, D.; Feigenson, G. W. *Biochim. Biophys. Acta* **2005**, 1746, 186.
- (18) Baumgart, T.; Hunt, G.; Farkas, E. R.; Webb, W. W.; Feigenson, G. W. *Biochim. Biophys. Acta* **2007**, 1768, 2182.
- (19) Sharonov, A.; Hochstrasser, R. M. *Proc. Natl. Acad. Sci. U.S.A.* **2006**, 103, 18911.
- (20) Betzig, E.; Patterson, G. H.; Sougrat, R.; Lindwasser, O. W.; Olenych, S.; Bonifacino, J. S.; Davidson, M. W.; Lippincott-Schwartz, J.; Hess, H. F. *Science* **2006**, 313, 1642.
- (21) Rust, M. J.; Bates, M.; Zhuang, X. *Nat. Methods* **2006**, 3, 793.
- (22) Widengren, J.; Seidel, C. A. M. *Phys. Chem. Chem. Phys.* **2000**, 2, 3435.
- (23) Gao, F.; Mei, E.; Lim, M.; Hochstrasser, R. M. *J. Am. Chem. Soc.* **2006**, 128, 4814.
- (24) Aramendia, P. F.; Krieg, M.; Nitsch, C.; Bittersmann, E.; Braslavsky, S. *Photochem. Photobiol.* **1988**, 48, 187.
- (25) Bernik DL, D. E. *Biochim. Biophys. Acta* **1993**, 1146, 169.
- (26) Yu, H.; Hui, S. *Biochim. Biophys. Acta* **1992**, 1107, 245.
- (27) Williamson, P.; Mattocks, K.; Schlegel, R. A. *Biochim. Biophys. Acta* **1983**, 732, 387.
- (28) Dragsten, P. R.; Webb, W. W. *Biochemistry* **1978**, 17, 5228.
- (29) Aiuchi, T.; Kobatake, Y. *J. Membr. Biol.* **1979**, 45, 233.
- (30) Salama, G.; Morad, M. *Science* **1976**, 191, 485.
- (31) Verkman, A. S.; Frosch, M. P. *Biochemistry* **1985**, 24, 7117.

- (32) Verkman, A. S. *Biochemistry* **1987**, 26, 4050.
- (33) Sato, C.; Nakamura, J.; Nakamaru, Y. *J. Biochem.* **2000**, 127, 603.
- (34) Ehrenberg, B.; Pevzner, E. *Photochem. Photobiol.* **1993**, 57, 228.
- (35) Kaschny, P.; Goni, F. M. *Eur. J. Biochem.* **1992**, 207, 1085.
- (36) Krumova, S. B.; Koehorst, R. B. M.; Bota, A; P ali, T; van Hoek, A; Garab, G; van Amerongen, H. *Biochim. Biophys. Acta* **2008**, 1778, 2823.
- (37) Bernik, D. L.; Disalvo, E. A. *Chem. Phys. Lipids* **1996**, 82, 111.
- (38) Bernik, D. L.; Tymczyszyn, E.; Daraio, M. E.; Negri, R. M. *Photochem. Photobiol.* **1999**, 70, 40.
- (39) Dodin, G.; Aubard, J.; Falque, D. *J. Phys. Chem.* **1987**, 91, 1166.
- (40) Dixit, N. S.; Mackay, R. A. *J. Am. Chem. Soc.* **1983**, 105, 2928.
- (41) Cremer, P. S.; Boxer, S. G. *J. Phys. Chem. B* **1999**, 103, 2554.
- (42) Schmidt, M. L.; Ziani, L.; Boudreau, M.; Davis, J. H. *J. Chem. Phys.* **2009**, 131, 175103.
- (43) Burns, A. R. *Langmuir* **2003**, 19, 8358

Schemes for Chapter 3:



Scheme 3.1. Kinetic Scheme for the Dimerization of MC540 Molecules in Liposomes

M_{\perp} is the monomer that is perpendicular to the membrane surface, $M_{//}$ is parallel to the membrane surface as described in the text, and M_2 represents the dimer of MC 540. The rate constants are from refs 31 and 32, and are only estimates for the present single molecule conditions

Figures for Chapter 3:

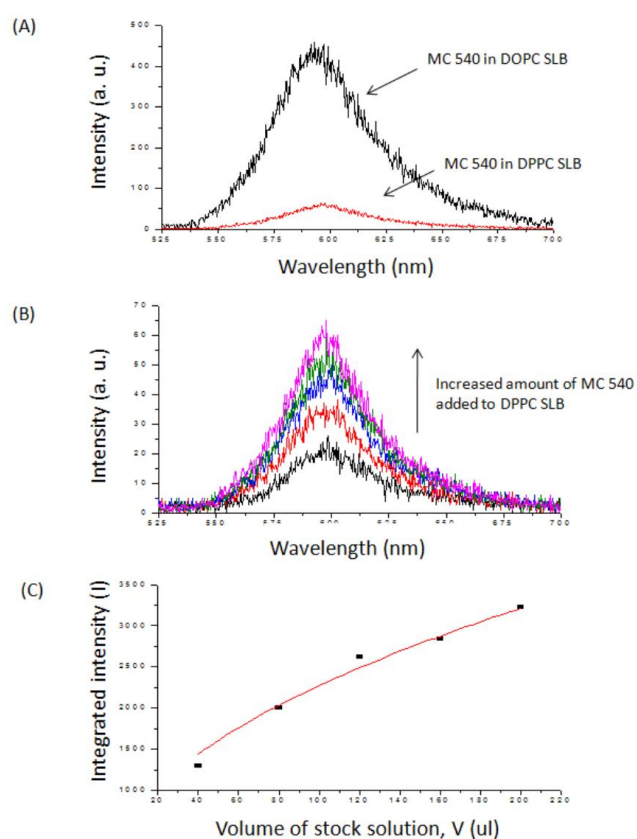


Figure 3.1. Fluorescence spectra of MC 540 in lipid bilayers.

(A) Fluorescence spectra of MC 540 (10^{-8} M) in DOPC SLB (black curve) or DPPC SLB (red curve) with 543.5 nm excitation. (B) Fluorescence spectra when increasing the volume (V) of MC 540 stock solution ($[MC\ 540] = 10^{-10}$ M) added to DPPC SLB ($[MC\ 540]$ by factors of 2 (lowest spectrum), 3, 4 to 5 fold (upper spectrum)). (C) Integrated fluorescence intensities (I) from (B), The red curve is the fit to the function $I = \text{constant } V^{1/2}$.

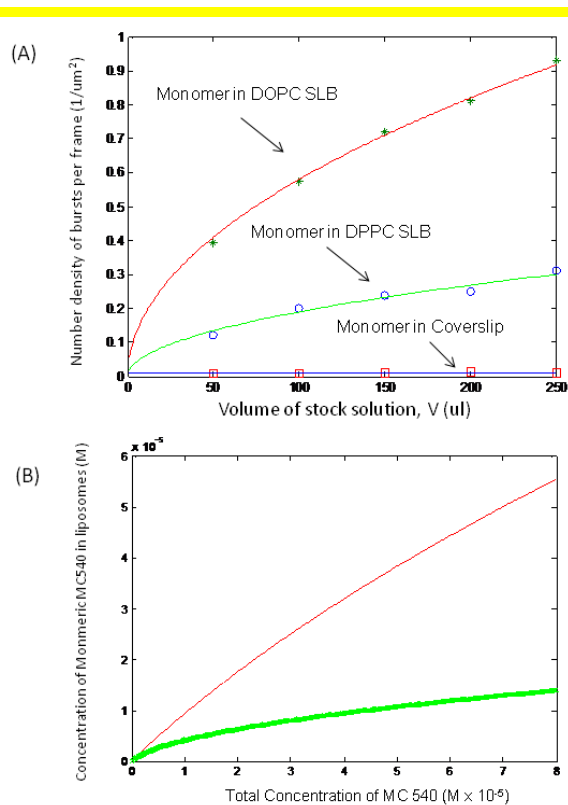


Figure 3.2. Comparison of populations of fluorescent monomers in the liquid and gel phases.

(A) Variation of the number density of single molecule bursts with volume of MC 540 solution ($[MC\ 540] = 10^{-10}$ M) added to solvent free DOPC SLB(*), DPPC SLB (\circ), or cleaned glass coverslip (\square). The red and green curves are the fits to the square root dependence on the total number of MC 540 molecules added. The blue curve shows there is no variation of the number density on the glass coverslips. The number density of single-molecule bursts on the cleaned glass coverslip was $\sim 0.01\ \mu\text{m}^{-2}$

(Continued figure 3.2) (B) Predicted MC 540 monomer concentration for liquid- (red curve) or gel- phase (green curve) phase liposomes as a function of total concentration of MC 540 based on the equilibrium dimerization constants for MC 540 ($K_d = 4 \times 10^3 \text{ M}^{-1}$ for liquid phase or $1.7 \times 10^5 \text{ M}^{-1}$ for gel phase liposomes^{31, 32, 37})

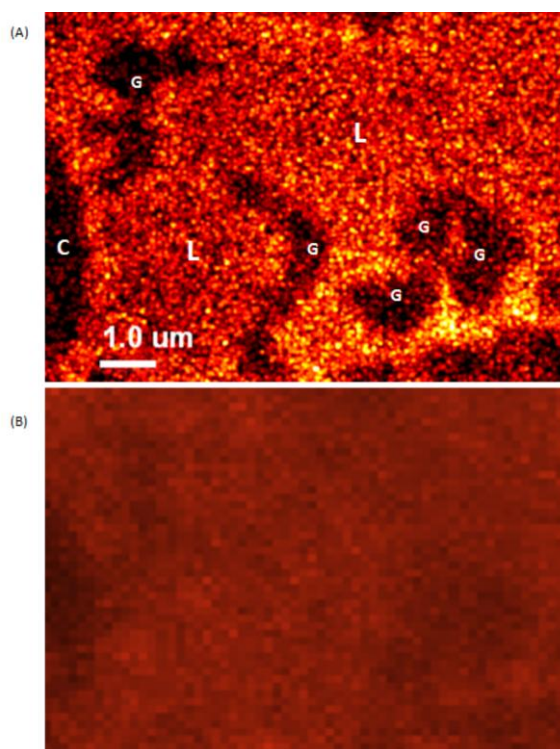


Figure 3.3. Comparison of PAINt and TIRFM images.

(A) Synthetic PAINt image from the coordinates of each single molecule burst of monomeric MC 540 on supported lipid bilayers (DOPC:DLPC=3:1). G denotes and highlights gel phase and L denotes liquid phase regions. (B) TIRFM images on the same region as (A) (sum of ~8000 frames). The PAINt method reveals the phase separation regions not seen in the TIRFM measurement. The PAINt procedure used to create image (A) eliminates spots that fail to satisfy criteria of sufficient photon number and aspect ratio¹⁹. These manipulations, combined with the loss of resolution and the difference in

(Continued from above) fluorescence intensity between gel and lipid phases, render image (B) more blurred than expected from simply a decrease in resolution.

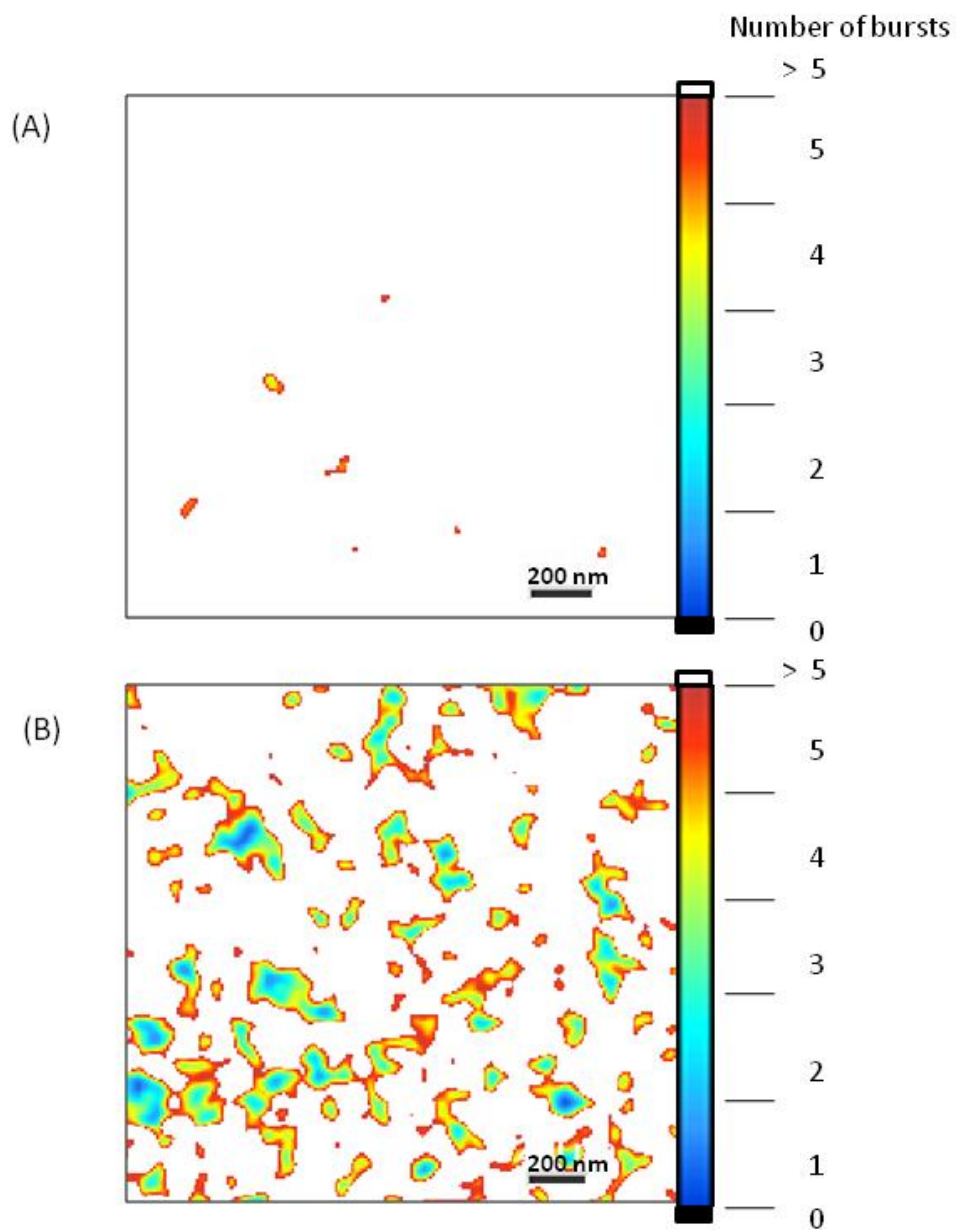


Figure 3.4. Comparison of Nile Red and MC 540 super-resolution images.

(A) Rainbow color mapped PAINT image of DOPC:DPPC=3:1 SLB with Nile Red as the probe. The gel and liquid phase regions are not resolved in the image.

(B) Rainbow color mapped PAINt image of the same region as the same sample in (A) using MC 540 as the probe. The nanoscale phase separation domains are clearly revealed in the image. Scale bar: 200 nm. When plotted using a full color scale, the image becomes spiky in the liquid-phase regions due to variations in the number of bursts per unit area and fails to reveal the nanoscale phase separation regions. Instead, the white color in the figure is used to represent those liquid regions with more than five bursts per unit area. The number density of bursts is 490 nm^{-2} .

Chapter 4 Monomer-Dimer Equilibrium of Merocyanine 540 Probed by Single Molecule Kinetic Studies

4.1 Introduction

Merocyanine 540 is known to be sensitive to lipid structure and voltage^{1,4}. Particularly, it has been widely employed as a probe for the measurement of membrane potentials⁵. It has been applied in epifluorescence microscopy to image phase domains in supported lipid monolayers³. Recently, it has been applied to image nanoscale phase separation⁶ of lipid bilayers with Point Accumulation in Nanoscale Topology (PAINT) method, previously developed by Sharonov and Hochstrasser⁷. It has been considered the emission characteristics of MC540 in various lipid phases and the membrane potential sensitivity come from the altered monomer-dimer equilibrium^{1, 8-10} and also distribution of two forms of monomer, parallel or perpendicular. Yet unambiguous evidence is still missing to support the conjecture that the equilibrium and two forms of monomers distinct the emission characteristics in various lipid phases. Therefore, we sought out to gather further supporting evidence for what is behind the scene of the emission species of MC540 in lipids of various phases by resorting to single molecule spectroscopy studies.

Webb et al.⁸ proposed that the voltage dependence of MC540 is associated with the equilibrium between monomers, oriented either parallel or perpendicular to membrane surface, and dimer (parallel to membrane surface) based on their polarization studies of MC540 in cholesterol bilayer membrane (see Scheme 4.1 for illustrative showing of

locations and orientations of monomers and dimers of MC540 in lipid membranes). Ever since their work, researchers^{1, 9, 11} have continued the idea that monomer dimer equilibrium is the main source of voltage sensitivity and lipid phase sensitivity. Verkman^{12, 13} et. al. did kinetic studies on MC540 in membranes to find out the binding kinetics of MC540 from aqueous solution to membranes, and the relative position and orientations of monomer and dimer. Bernik^{2, 11, 14} et. al. performed a series of photophysical studies on MC540 in lipid or gel phase. In short, their findings suggested that the monomeric form of MC540 resides close to the lipid head group, and monomers are in large perpendicular to the membrane surface (M_{\perp}). To form an anti-parallel dimer, the monomers have to migrate to a deeper position in the membrane and reorient itself into a parallel form of MC540 (M_{\parallel}). The dimers (M_2 or D) are parallel to membrane surface and in a position closer to the surface compared to the perpendicular monomers (see Scheme 4.1 for illustration of the relative positions and orientation of monomers and dimers in membrane). The monomers absorb at 570 nm and emit at 590 nm^{1, 10, 15}. The fluorescent quantum yield of monomeric MC540 is reported as 0.6 in lipid environment, while it is 0.05 in aqueous surroundings⁴. In contrast, the dimeric form of MC540 in liposomes absorbs at 540 nm and emits with a fairly low, yet noticeable quantum yield only in the gel phase^{2, 11, 14}.

It is therefore quite intuitive to conclude as in the previous chapter and in the scheme 3.1, that the perpendicular monomer of MC540 is the emitting species (or say, the on states) of the bursts, while the dimers are responsible for the off states as the bursts disappear. However, since MC540 as a probe combined with the PAINT method serves

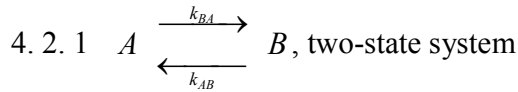
as the first example for phase sensitive super-resolution microscopy, it is worthwhile to gather more concrete evidence for the emitting species and the underlying kinetics leading to the on and off states. To achieve this goal we resort to kinetic studies on the single molecule level and polarization dependent imaging.

4.2 Single molecule kinetics

Single molecule kinetic study based on fluorescent intensity time records has been a powerful tool¹⁶⁻²⁰ to remove the ensemble average, and gather detailed information regarding static and dynamic heterogeneity, transition between different function states, probability distribution function, and evaluation of kinetic scheme of a system. The recent progress of single molecule kinetics advances is given in the chapter 1. The background of possible kinetic schemes for the analysis of intensity-time trajectories is provided here to serve as a basis for further discussion. The unit for discussion of chemical kinetics on single molecule level is the time-dependent probability of a single molecule dwelling in a specific chemical state, rather than the concentration of chemical species. Four possible kinetic schemes (Scheme 4.2) are discussed in the following. The prediction of the on-time (τ_{on}) and off-time (τ_{off}) probability distributions for these kinetic schemes is given as below.

As previously introduced in chapter 1, for intensity-time fluorescent trajectories, the fluorescent signals constantly jumps between background and certain signal level. The trajectory would appear as a series of fluorescent bursts in between dark periods. The lengths of both fluorescent bursts and dark periods are stochastic, and yet they are

associated with the underlying kinetics that guide the switching between on and off states. The experimental values of τ_{on} , τ_{off} , and the probability distributions can be obtained from the intensity time trajectories. The trajectories can also be evaluated by theoretical prediction^{20-23, 23, 24, 24-28} based on the proposed kinetic schemes and the rate constants of each half reaction.



For the single molecule scheme $A \xrightleftharpoons[k_{AB}]{k_{BA}} B$, the system jumps between states A

and B stochastically with forward rate constant k_{BA} and backward rate constant k_{AB} .

Assuming that state A is the fluorescent state (on state) and B is non-fluorescent state (off

state), the system following the kinetic scheme of $A \xrightleftharpoons[k_{AB}]{k_{BA}} B$ will appear switching

between on and off state stochastically. The rate equations for the kinetic scheme are as the following:

$$\begin{aligned} \frac{dC_A(t)}{dt} &= -k_{BA}C_A(t) + k_{AB}C_B(t) \\ \frac{dC_B(t)}{dt} &= k_{BA}C_A(t) - k_{AB}C_B(t) \end{aligned}$$

where $C_A(t)$ and $C_B(t)$ are the time-dependent amount of molecules of the system being in the fluorescent state A and non-fluorescent state B, respectively. If we are aware of the total amount of molecules added into the system, then we may divide these equation with $C_T = C_A(t) + C_B(t)$. The equations become

$$\frac{df_A(t)}{dt} = -k_{BA}f_A(t) + k_{AB}f_B(t)$$

$$\frac{df_B(t)}{dt} = k_{BA}f_A(t) - k_{AB}f_B(t)$$

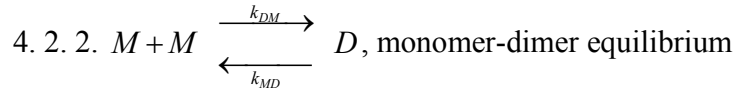
$f_A(t)$ and $f_B(t)$ are the time-dependent probability of the system being in the fluorescent state A and non-fluorescent state B, respectively. The forward rate constant is k_{BA} and the backward rate constant is k_{AB} . To predict τ_{on} and τ_{off} distributions, the corresponding half reactions shall be considered as below. The τ_{on} distribution $P_{on}(t)$ is termed the on-time probability density distribution function and can be determined by considering: $P_{on}(t)\Delta t$ is the probability for the system to switch from on state to off state at time t , which yields $P_{on}(t)\Delta t = \Delta f_B(t)$ (gained probability of system switching to state B from state A). Then $\Delta f_B(t) = k_{BA}f_A\Delta t$ stands because of the $A \xrightarrow{k_{BA}} B$ half reaction. Based on the $A \xrightarrow{k_{BA}} B$ half reaction, $\frac{df_A(t)}{dt} = -k_{BA}f_A(t)$, $f_A(t) = e^{-k_{BA}t}$, so $P_{on}(t) = k_{BA}e^{-k_{BA}t}$. Similarly,

$P_{off}(t) = k_{AB}e^{-k_{AB}t}$ can be obtained. Therefore, the above results show that both $P_{on}(t)$ and

$P_{off}(t)$ for the kinetic scheme $A \xrightleftharpoons[k_{AB}]{k_{BA}} B$ would exhibit single exponential decays with

rate constants of k_{BA} and k_{AB} . The mean on-time $\langle \tau_{on} \rangle$ and mean off-time $\langle \tau_{off} \rangle$ can be

obtained by using $\langle \tau_{on} \rangle = \int t P_{on}(t) dt = \frac{1}{k_{BA}}$, and $\langle \tau_{off} \rangle = \int t P_{off}(t) dt = \frac{1}{k_{AB}}$.



The rate equations for the kinetic scheme are

$$\begin{aligned} \frac{dC_M(t)}{dt} &= -k_{DM}C_M^2(t) + 2k_{MD}C_D(t) \\ \frac{dC_D(t)}{dt} &= -k_{MD}C_D(t) + \frac{1}{2}k_{DM}C_M^2(t) \end{aligned}$$

where $C_M(t)$ and $C_D(t)$ are the time-dependent amount of the system being in the fluorescent state M and non-fluorescent state D, respectively. In the kinetic scheme, all monomers are deemed equal. That is, they all emit with the same quantum yield after they are excited while dimers are responsible for the dark periods. By introducing C_T (total population of merocyanine 540 molecules added to the system) as $C_T = C_M + 2C_D$ (all merocyanine 540 molecules added are either in monomeric or dimeric form as they bind to the lipids), the rate equations can be rewritten as:

$$\begin{aligned} \frac{df_M(t)}{dt} &= -k_{DM}C_T f_M^2(t) + 2k_{MD}f_D(t) \\ \frac{df_D(t)}{dt} &= -k_{MD}f_D(t) + \frac{1}{2}k_{DM}C_T f_M^2(t) \end{aligned}$$

where C_T is a time-independent entity since total amount of the molecules in the system is fixed (because we do know how many molecules we add in the system, therefore it does not vary with time), and $f_M(t)$ and $f_D(t)$ are the time-dependent probability of the system being in the fluorescent state M and non-fluorescent state D, respectively. Precisely, $f_M(t) = C_M(t)/C_T$ and $f_D(t) = C_D(t)/C_T$. It follows that $P_{on}(t)\Delta t = f_M(t)\Delta t = k_{DM}f_T f_M^2(t)\Delta t$ and therefore $P_{on}(t) = k_{DM}C_T f_M^2(t)$. From the half

reaction $M + M \xrightarrow{k_{DM}} D$, one can get $f'_M(t) = -k_{DM}C_T f_M^2(t)$, and hence

$$f_M(t) = \frac{1}{k_{DM}C_T t - Const}. \text{ It follows that } P_{on}(t) = \frac{1}{2}k_{DM}C_T \frac{1}{(k_{DM}C_T t - Const)^2}.$$

Since the integrated probability of probability density function of the on times should be one, one may use

$$\int_0^{\infty} P_{on}(t) dt = 1 = \frac{1}{2} \int_0^{\infty} k_{DM}C_T \left[\frac{1}{(k_{DM}C_T t - Const)^2} \right] dt \quad \text{to get}$$

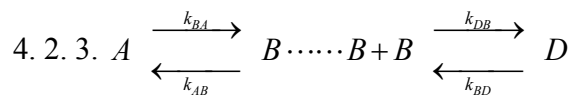
$$1 = -\frac{1}{2k_{DM}C_T - Const} \Rightarrow Const = -\frac{1}{2k_{DM}C_T}. \quad \text{Therefore,}$$

$$P_{on}(t) = \frac{1}{2}k_{DM}C_T \frac{1}{\left(k_{DM}C_T t + \frac{1}{2k_{DM}C_T}\right)^2} \quad \text{and} \quad \langle \tau_{on} \rangle = \int_0^{\infty} t P_{on}(t) dt. \quad \text{Similarly,}$$

$P_{off}(t)\Delta t = f'_D(t)\Delta t = k_{MD}f_D(t)\Delta t$ holds true for the off time probability distribution function. From the half reaction $M + M \xleftarrow{k_{MD}} D$, one can get $f_D(t) = e^{-k_{MD}t}$. Therefore,

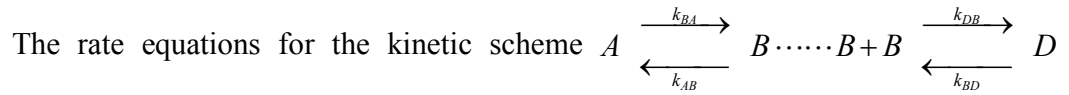
$$P_{off}(t) = k_{MD}e^{-k_{MD}t} \text{ and } \langle \tau_{off} \rangle = \int_0^{\infty} t P_{off}(t) dt = \frac{1}{k_{MD}}.$$

The off-time probability distribution function for the kinetic scheme would follow a single exponential decay function and the mean off-time would be $1/k_{MD}$.



Even though from the scheme and discussions from the previous chapter, it seems that making the assumption that state A is the fluorescent state and is from the

perpendicular (to lipid membrane surface) form of monomeric MC540 with B being the parallel form of monomeric MC540, and D being the dimeric form. Both B and D are the dark, non-fluorescent states. Here such assumption is not applied so that the analysis based on the kinetic scheme can be used to help examine what form of monomeric MC540 shall be deemed responsible for the fluorescent bursts in the phase sensitive nanoscale super-resolution microscopy in the previous chapter. Therefore, here we only assume that state A, the fluorescent state, is one form of monomeric MC540, and it does not directly link to the formation of dimers, state D. Formation of dimers has to go through another non-fluorescent state B, which is another form of the monomers.



would be

$$\begin{aligned}\frac{dC_A(t)}{dt} &= -k_{BA}C_A(t) + k_{AB}C_B(t) \\ \frac{dC_B(t)}{dt} &= -k_{AB}C_B(t) + k_{BA}C_A(t) - k_{DB}C_B^2 + 2k_{BD}C_D(t) \\ \frac{dC_D(t)}{dt} &= \frac{1}{2}k_{DB}C_B^2 - k_{BD}C_D(t)\end{aligned}$$

with $C_A(t)$, $C_B(t)$ and $C_D(t)$ being the time-dependent amount of molecules of the system being in the fluorescent state A, non-fluorescent state B and D, respectively. Here we introduce the time-independent constant $C_T = C_A + C_B + 2C_D$. The rate equations can be rewritten as

$$\begin{aligned}\frac{df_A(t)}{dt} &= -k_{BA}f_A(t) + k_{AB}f_B(t) \\ \frac{df_B(t)}{dt} &= -k_{AB}f_B(t) + k_{BA}f_A(t) - k_{DB}C_T f_B^2 + 2k_{BD}f_D(t) \\ \frac{df_D(t)}{dt} &= \frac{1}{2}k_{DB}f_B^2 - k_{BD}f_D(t)\end{aligned}$$

where $f_A(t)$, $f_B(t)$ and $f_D(t)$ are the time-dependent probability of the system being in the fluorescent state A, non-fluorescent state B and D, respectively. Here $f_A(t) = C_A(t)/C_T$, $f_B(t) = C_B(t)/C_T$ and $f_D(t) = C_D(t)/C_T$. It follows that

$$\begin{aligned}P_{on}(t)\Delta t &= -\Delta f_A(t) = k_{BA}f_A(t)\Delta t = -\frac{df_A}{dt}\Delta t \\ \Rightarrow \frac{df_A}{dt} &= -k_{BA}f_A \dots \Rightarrow f_A(t) = e^{-k_{BA}t} \\ P_{on}(t) &= k_{BA}e^{-k_{BA}t}\end{aligned}$$

and therefore $\langle t_{on} \rangle = \frac{1}{k_{BA}}$. The on-time probability distribution function for the kinetic scheme would be single exponential decay functions. For the off-time probability distribution function, one can get

$$\begin{aligned}P_{off}(t)\Delta t &= \Delta f_A(t) = k_{AB}f_B(t)\Delta t \\ P_{off}(t) &= k_{AB}f_B\end{aligned}$$

f_B is associated with the following differential equations

$$\begin{aligned}f_B' &= -k_{AB}f_B - k_{DB}C_T f_B^2 + 2k_{BD}f_D \\ f_D' &= \frac{1}{2}k_{DB}C_T f_B^2 - k_{BD}f_D\end{aligned}$$

However, there is no exact analytical solution for f_B . One can obtain the numerical solution for f_B using constants in the differential equations associated with different initial

conditions. If we assume we can distinguish how the initial conditions are, we may work out numerical solutions for various initial conditions. For example, if we assume that the system starts with the total population being in the non-fluorescent state B (that is, $f_B(0)=1, f_C(0)=0$), we can use such initial condition to obtain the numerical solution of f_B^B by numerically solving the differential equation in any given mathematical softwares. Here we denote such initial condition where initially the system is in the state B by adding a symbol B as a superscript. Similarly, by using the initial condition of $f_B(0)=0, f_C(0)=1$, we can obtain f_B^C . Therefore, we can still get numerical value for the probability distribution function of the off times by assigning different initial conditions. For the two initial conditions we discussed above, by numerically solving the differential equations, we can get

$$P_{off}^B = k_{AB} f_B^B (f_B(0)=1, f_C(0)=0)$$

$$P_{off}^C = k_{AB} f_B^C (f_B(0)=0, f_C(0)=1)$$

where the superscript denotes where the population of the system initially is. Furthermore, if we are aware of how the equilibrium population of the system being in the non-fluorescent state B or C, then we can get the numerical value of the probability distribution function of the off-time at any given time by using $P_{off}(t) = P_B^{eq} P_{off}^B(t) + P_C^{eq} P_{off}^C(t)$ where the superscript *eq* denotes the population at equilibrium. This way, one can still get mean off-time and off-time probability distribution function. Below we take this further by going over how one can get the values of the rate constants needed to numerically solve the differential equation.

Starting with the dimerization equilibrium constant K_d ,

$$K_d = \frac{C_D}{(C_A + C_B)^2}$$

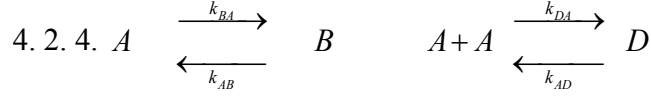
one can assume the system is at equilibrium and therefore $\frac{dC_A}{dt} = 0 = \frac{dC_B}{dt} = \frac{dC_D}{dt}$. This,

combined with the above differential equations of the kinetic scheme, will give that

$$\begin{aligned} k_{BA} C_A &= k_{AB} C_B; & k_{DB} C_B^2 &= k_{BD} C_D \\ C_A &= \frac{k_{AB}}{k_{BA}} C_B; & C_D &= \frac{k_{DB} C_B^2}{k_{BD}} \\ K_d &= \frac{\frac{k_{DB} C_B^2(t)}{k_{BD}}}{\left(1 + \frac{k_{AB}}{k_{BA}}\right)^2 C_B^2(t)} = \frac{k_{DB}}{k_{BD}} \frac{1}{\left(1 + \frac{k_{AB}}{k_{BA}}\right)^2} \\ k_{DB} &= k_{BD} \left(1 + \frac{k_{AB}}{k_{BA}}\right)^2 K_d \end{aligned}$$

Therefore, given the ratio of the different form of monomers and the dimerization constants, one can get the parameters needed to numerically evaluate the off-time probability distribution function. To give a brief idea what the off-time probability distribution function would behave for the kinetic scheme, we give the numerical solution here. By using rate constants and parameters that fit our experimental conditions, typical off-time probability distribution function for the kinetic scheme shows a profile that resemble a decay function with two exponential component, short one below 3 ms and long one around tenths of ms. The mean off-time ranges around 10 ms to over a

hundred milliseconds. The exact results of the numerically solved off-time probability distribution functions will be shown in section 4.3.



Similar to the assumptions we made in 4.2.3. Both B and D are the dark, non-fluorescent states. Here we assume that state A, the fluorescent state, is one form of monomeric MC540, and it directly links to the formation of dimers, state D. Formation of dimers does not go through another non-fluorescent state B, which is another form of the monomers.

The rate equations for the kinetic scheme would be

$$\begin{aligned} \frac{dC_A(t)}{dt} &= -k_{BA}C_A(t) + k_{AB}C_B(t) - k_{DA}C_A^2 + 2k_{AD}C_D(t) \\ \frac{dC_B(t)}{dt} &= k_{BA}C_A(t) - k_{AB}C_B(t) \\ \frac{dC_D(t)}{dt} &= \frac{1}{2}k_{DA}C_A^2 - k_{AD}C_D(t) \end{aligned}$$

with $C_A(t)$, $C_B(t)$ and $C_D(t)$ being the time-dependent amount of molecules of the system being in the fluorescent state A, non-fluorescent state B and D, respectively. Here we introduce the time-independent constant $C_T = C_A + C_B + 2C_D$. The rate equations can be rewritten as

$$\begin{aligned} \frac{df_A(t)}{dt} &= -k_{BA}f_A(t) + k_{AB}C_B(t) - k_{DA}C_T C_A^2 + 2k_{AD}f_D(t) \\ \frac{df_B(t)}{dt} &= k_{BA}f_A(t) - k_{AB}f_B(t) \\ \frac{df_D(t)}{dt} &= \frac{1}{2}k_{DA}C_T f_A^2 - k_{AD}f_D(t) \end{aligned}$$

where $f_A(t)$, $f_B(t)$ and $f_D(t)$ are the time-dependent probability of the system being in the fluorescent state A, non-fluorescent state B and D, respectively. Here $f_A(t) = C_A(t)/C_T$, $f_B(t) = C_B(t)/C_T$ and $f_D(t) = C_D(t)/C_T$. It follows that

$$P_{on}(t)\Delta t = -\Delta f_A(t) = \left[k_{DA}f_A(t) + k_{DA}C_T f_A^2 \right] \Delta t$$

$$f_A' = -k_{BA}f_A - k_{DA}C_T f_A^2$$

. If $f_A(0)$ is known, then the analytical solution for f_A is

$$f_A(t) = \frac{k_{BA}f_A(0)}{\left[(k_{BA} + k_{DA}C_T f_A(0))e^{k_{BA}t} - k_{DA}C_T f_A(0) \right]}$$

The on-time probability distribution function for the kinetic scheme would be

$$P_{on}(t) = \frac{k_{BA}^2}{\left[(k_{BA} + k_{DA}C_T f_A(0))e^{k_{BA}t} - k_{DA}C_T f_A(0) \right]} + \frac{C_T f_A(0) k_{BA}^2 k_{DA}}{\left[(k_{BA} + k_{DA}C_T f_A(0))e^{k_{BA}t} - k_{DA}C_T f_A(0) \right]^2}$$

To find mean on-time, one can use

$$\langle t_{on} \rangle = \int_0^{\infty} t P_{on} dt = \frac{\ln \left(\frac{k_{BA} + k_{DA}C_T f_A(0)}{k_{BA}} \right)}{k_{DA}C_T f_A(0)}$$

If $k_{DA}C_T f_A(0)/k_{BA} \ll 1$, then the mean on-time simplifies to $\langle t_{on} \rangle = \frac{1}{k_{BA}}$. For the off-time

probability distribution function, one can get

$$P_{off}(t) = \Delta f_A(t) = \left[k_{AB}f_B(t)f_B^{eq} + k_{AD}f_D(t)f_D^{eq} \right] \Delta t$$

$$\Rightarrow P_{off}(t) = k_{AB}f_B(t)f_B^{eq} + k_{AD}f_D(t)f_D^{eq}$$

, where f_B^{eq} denotes the probability of the system being in the non-fluorescent state B at equilibrium. f_B and f_C can be solved by the following differential equations

$$\begin{aligned}\frac{df_B(t)}{dt} &= -k_{AB}f_B(t) \\ \frac{df_D(t)}{dt} &= -k_{AD}f_D(t)\end{aligned}$$

The off-time probability distribution function has two exponential decay components and is as follows:

$$P_{off}(t) = k_{AB}f_B^{eq}e^{-k_{AB}t} + k_{AD}f_D^{eq}e^{-k_{AD}t}$$

So the mean off-time would be $\langle t_{off} \rangle = \frac{f_B^{eq}}{k_{AB}} + \frac{f_D^{eq}}{k_{AD}}$ where f_B^{eq} (f_D^{eq}) stands for the equilibrium probability of the system being in state B (D).

4.3 Results

On a glass surface, Merocyanine 540 were used as probes to image individual nonfluorescent lipid (DLPC, DPPC, or DMPC) vesicles (~ 100 nm in diameter), as shown in Figure 4.1. Figure 4.1 displays a typical scanning fluorescence image of a glass coverslip covered by properly adjusted amount of lipid vesicles with MC540 as the probe. The surface density of vesicles is adjusted so that each vesicle is well separated from another vesicle by several hundreds of nanometers (\sim diffraction limited distance). The fluorescence spots in Figure 4.1 are proven to be the results of the interaction between Merocyanine 540 and lipid vesicles immobilized on glass (see spectra in Figure 4.2). All the preparation procedures for samples and instrumental details can be found in chapter 2.

The bulk spectra of the fluorescent spots are consistent with those of Merocyanine 540 monomers bound to lipid vesicles^{11,29}. The same glass surface in the presence of either a similar MC540 solution or a lipid vesicle solution proves to have no observable fluorescence in our experiments. The absorption and fluorescence of MC540 in aqueous and nonpolar lipid environments are distinctive. It emits weakly in aqueous solution compared with lipid (~20 fold increase of quantum yield). Such characteristic enables single molecule experiments on lipid-bound probes owing to low background interference from the solution. The average diameter of the vesicles used in the experiments is ~100 nm, which is much smaller than the $1/e^2$ width of the focused laser beam, 500-600 nm. Therefore, most of the fluorescence spots in Figure 4.1 appear as if they were single molecules.

These fluorescence spots constantly switches on and off in between different scans. As a signature of single molecule images, each spot does not appear as a merely round diffraction limited bright spot; it appears as a stripe-filled diffraction limited object with the stripe pattern varies from time to time. This characteristic comes directly from the fast scanning through single molecule fluorescent spots with various on and off intensity-time trajectory. The emission spectra (Figure 4.2) match those reported for monomeric MC540 in lipids. The concentration used in these fluorescence spectra measurements was 10 times higher than in the single molecule intensity-time trajectory measurements to provide a reasonable signal-to-noise for display. Only monomer fluorescence was seen in all three kind of lipids used in our experiments.

By zooming into the region where a fluorescence spot is located, a fluorescence intensity-time record can be obtained by binning the signal counts versus time variable. The record is composed of sequential bursts of fluorescence photons segregated by relatively longer dark periods as there is no emission. Typical intensity-time trajectories with various time spans for a MC540 bound DMPC vesicle are displayed in Figure 4.3. MC540 bound DPPC and DLPC vesicles show similar trajectories. The system becomes fluorescent every few tenth of ms and stays for a few ms and then switches off. By properly adjusting the concentration and the amount of stock solution of MC540 added into the sample solution, the off-time can be adjusted to vary from 10 to around 100 ms to make the observation of fluorescence spots, the acquisition of intensity time trajectories, and comparison of various kinds of lipids bound with MC540 easier. The concentration of the stock solution of MC540 used for DLPC, DMPC, DPPC vesicles are $7.5 \times 10^{-7} \text{M}$, $7.5 \times 10^{-7} \text{M}$, and $7.5 \times 10^{-7} \text{M}$, respectively. The reasoning of why different concentration of probe stock solution for different lipid and how it can be linked to the underlying monomer-dimer equilibrium of MC540 in lipids will be presented in the following sections (4.3 and 4.4).

To determine the widths of the fluorescence bursts and the corresponding dark periods of in the intensity-time trajectories, the following data analysis procedure is used. Each intensity-time trajectory is used without applying any smoothing filter. A threshold was carefully selected and a home-made Matlab program is used to extract the fluorescence burst widths (on-times) and the lengths of the dark periods (off-times), as shown in Figure 4.3. The burst width is the time interval as the continuous fluorescence

signal is above the selected threshold. The dark period is the time interval as the signal is below the threshold. Figure 4.4 displays typical on-time and off-time distributions associated with MC540 bound DLPC, DMPC, and DPPC vesicles on glass surface, respectively. The red curve shows exponential decay fitting to the distributions. In our experiments, three kind of lipids and five volumes of the probe stock solution are used to gather information of various amount of MC540 molecules in different kind of lipids. Over 250 trajectories of 120 seconds in length are collected for each lipid and volume of the probe stock solution added. The mean on-time and off-time associated with each vesicle are then used to generate the distribution of mean on-times and mean off-times averaging over many vesicles. Figure 4.5 displays the average on-time and off-time for varying amount of probe stock solution added in different kind of lipids. The average on-time shows no variation for different amount of probe stock solution added for each kind of lipids. On the contrary, the average off-time rate (inverse of the average off-time) shows a linear increase as the amount of probe stock solution added to the system increases for all three kinds of lipids. The detailed discussion and analysis on how the on-time and off-time varies with the concentration and the amount of stock solution for different lipid will be given in the following section. It is worth noting that in Nile Red bound vesicle intensity time trajectories²², the average off-time rate (inverse of average off time) would not show any change unless there is a change in solution concentration (see the dashed line in Figure 4.5), while the change of the average off-time for MC540 bound vesicles shows that whatever kinetic scheme is going on behind the formation of

the intensity time trajectory does not involve molecules in the solution but only takes places in the lipid vesicles.

Figure 4.6 (A) shows a typical simulated off-time probability distribution by using the kinetic scheme 4.2.3. It shows a bi-exponential decay profile and the average off-time falls in the range of 10-100 ms similar to our experimental results. The typical parameters used for the simulations are k_{AB} from 600 to 2000 s^{-1} , $k_{DB}C_T$ from 4000 to 90000, $K_d=4 \times 10^3 M^{-1}$ for MC540 in liquid phase, $1.7 \times 10^5 M^{-1}$ in gel phase, and $k_{AB}/k_{BA}= 6$ for liquid phase; 1.5 for gel phase¹⁰. The difference in the amount of MC540 added in the system (volume of stock solution added) comes in from altering P_B^{eq} and P_D^{eq} . Figure 4.6 (B) shows the predicted average off-time from various kinetic schemes and its variation with increased volume of stock solution added in the system.

Figure 4.7 (A) displays the synthesized polarization dependent PAINt images of nanosized lipid bilayer wrapped silica (100 nm in size) and figure 4.7B shows the comparison of the number density distribution of points in either the x or y directional cross section on the synthesized PAINt image using s-polarized, p-polarized, or circularly polarized excitation. The membrane wrapped nanosized silica, instead of large unilamellar vesicles, is used here because the sphere shape of the membranes is well preserved due to the support of the nanosized silica. Therefore, the orientation of the dipole moments of molecules of perpendicular or parallel monomers of MC540 can stay in line with either the norm or the surface of the sphere. The experimental procedure used to gather the PAINt image in Figure 4.7A is the same as the one used before (Chapter 3) except that either s-Polarized or p-Polarized beam, instead of circularly polarized beam,

is used to excite the sample. The cross-sectional distribution of centroid points of single molecules on the sphere under different polarization condition can be used to narrate the preference of the orientation of the dipoles of MC540 molecules. This will be detailed in the following discussion section.

Figure 4.8 shows the wide-field fluorescent images of MC540 bound giant unilamellar vesicles (DLPC) under polarized excitation. The arrow indicates the polarization direction of the incident light and as can be seen in Figure 4.8, the bright edges on the circle are perpendicular to the polarization direction. This indicates that the dipole moment of the MC540 molecules responsible for the emission lies perpendicular to the membrane surface. Discussion on this front will be detailed in the following section.

4.4 Discussion

The following discussion will be focused on linking the corresponding kinetics of monomeric and dimeric forms of MC540 and the single molecule fluorescent spots observed in the phase sensitive PAINt microscopy in the previous chapter. Before we go further into that, we will discuss a bit regarding some basic aspects about spectroscopic features and sample characteristics of MC540 bound large unilamellar vesicles.

One distinguishing feature regarding the binding between MC540 molecules and lipid vesicles is that once they get into lipid vesicles, it is very rare for the molecules to get released into solution from the vesicles. Therefore, it is fairly important to adjust the initial condition properly because if too many molecules are bounded to vesicles it is

nearly impossible to get them to become unbound from the vesicles. This is very different from the property of common probes in microscopic use. For example, the amount of Nile Red²² molecules for PAINT microscopy can be adjusted at will. The concentration of probes is linked to the association of the dyes and vesicles in the Nile Red case. The association kinetics affects the average off times of the intensity time trajectories of Nile Red bound vesicles. Therefore, without alteration of the concentration of Nile Red, there would be no variation of the average off times. However, this is not the case for MC540 bound LUVs. What we found, both in the previous chapter and experiments presented in this chapter, is that even the same MC540 stock solution of the same concentration is added into the solution, the average off-times will be affected (to be detailed in 4.4.1). What it says is that the amount of MC540 molecules bounded to the vesicles, instead of the concentration of MC540 in solution alone, is affecting the blinking features of the single molecule fluorescent spots. This is further supported either by exchanging the solution with water or by sucking the solution out of the sample vial and leaving just the vesicles on the glass coverslip. For Nile Red bound vesicles²², this would lead to diminishing signal counts and difficulty in locating fluorescent dye-bound vesicles. However, for MC540 bound vesicles, no obvious decrease in the signal intensities of the fluorescent spots is observed. All the above findings show that whatever is responsible for the blinking features of the MC540 bound vesicles is going on in the vesicles rather than through interactions between species in and out the vesicles. To make the observation more evident, we conducted all the intensity time trajectory experiment by

varying the amount of the stock solution added in the solution (hence the amount of molecules in lipids) rather than simply varying the concentration of the solution.

On the spectroscopic feature of MC540 bound vesicles, as can be seen in Figure 4.2, all three spectra of MC540 in DLPC, DMPC, and DLPC show peaks around 590 nm, which is linked to monomeric MC540 conventionally^{1,9}. The monomeric form of MC540 in liposomes absorbs at 570 nm and emits at 590 nm. Dimeric MC540 in liposomes absorbs at 540 nm and emits with low yield (only in gel phase lipids, it is nearly non-fluorescent in other phases of lipids) at 625 nm. The concentration used for the emission spectra in Figure 4.2 is 10 times higher than in the intensity-time trajectory collection to give a reasonable signal-to-noise ratio. No emission peak around 625 nm (which indicates dimeric MC540 emission) has been observed, even when the concentration of MC540 is 100 times higher than in the intensity-time trajectory collection. Therefore, the fluorescent state (on-state) of the intensity time trajectory in Figure 4.3 can be attributed to from the monomeric MC540 emission. Note we do not specify which form (perpendicular or parallel) of MC540 is responsible for the emission yet. To further ensure only monomeric MC540 is collected in our experiments, the optics (filter sets) were properly selected so that only emission from 580 to 625 nm is windowed to yield intensity time trajectories for our analysis.

4.4.1 Analysis of the intensity-time trajectories of MC540 bound lipid vesicles

From Figure 4.3, one can see there are bursts (fluorescent states) with signal counts above 20 (counts per millisecond) and background (non-fluorescent states) with signal

around 5 (c.p.s). For all three kind of lipids used in our studies (DLPC, DMPC, and DPPC), the fluorescent states stay being fluorescent for around 3 ms and goes off. The time scale of the current system being in the fluorescent state coincides well with the survival time of perpendicular monomeric MC540 according to the typical kinetic parameters and the kinetic scheme provided in the last chapter. The length of the non-fluorescent states varies with the amount of MC540 molecules present in the lipid vesicles. By properly controlling the stock solution concentration of MC540, we were able to get the average off time to be within 10 to 100 ms window. Each off time presents in each trajectory varies stochastically. By setting an appropriate selection level (20 c.p.s., for example) and applying the threshold to differentiate the trajectory into respective on-states and off-states, we can sort a trajectory into collections of on-times and off-times. It shows no measurable correlation from single vesicle results either between on-times and the following off-times or between two successive on-times and/or off-times. The same result hold true for analysis after averaging over 200 vesicles all together. Therefore, all the information regarding the kinetic schemes of MC540 bound vesicles behind the on and off switching patterns is contained in the respective on- and off-time distribution function, from which the intensity-time trajectory can be reconstructed. As can be seen in Figure 4.4, the fluorescence burst widths and dark periods associated with each vesicle are then used to generate the probability distribution function of on-time and off-time. For all three kinds of lipids and various amounts of MC540 in the vesicles used in our study, the on-time distributions followed a single exponential decay. The off-time distribution shows doubly exponential decays having a short component smaller than or

around 1ms and a longer component from 10 to 100 ms in accordance with the decrease of amount of MC540 molecules in vesicles. By averaging the mean on-time and mean off-time from each vesicle, one can get the average on-time and off-time for each lipid and amount of MC540 presented in the system (as can be seen in Figure 4.5). What it shows in Figure 4.5 is that the average on-time for DLPC, DMPC, or DPPC is 3 ms, 2.6 ms, or 2.6 ms, respectively and no variation with the amount of MC540 in vesicles is observed while the average off-time for three kinds of lipids decrease from 100 ms to 10 ms according to the increase of the amount of MC540 in the system. That is, the average on-time is concentration independent and the average off-time varies with numbers of MC540 in the system.

Now we can come back to the previous analysis (see section 4.2 for details) of potential kinetic schemes of MC540 monomer-dimer equilibrium.

A simple two state kinetic scheme $A \xrightleftharpoons[k_{AB}]{k_{BA}} B$ is ruled out since the average off-

time follows as $\langle \tau_{off} \rangle = \int t P_{off}(t) dt = \frac{1}{k_{AB}}$ (see section 4.2.1 for the deductions) and hence

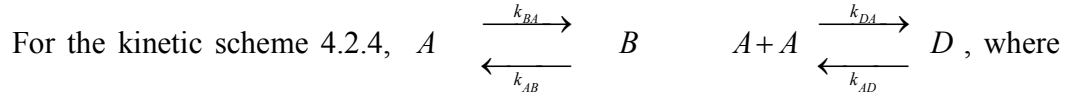
is concentration independent. Therefore, any more complicated scheme that is reducible²⁷ to the two state kinetic scheme can also be rejected.

As for the kinetic scheme 4.2.2 $M + M \xrightleftharpoons[k_{MD}]{k_{DM}} D$, the average off-time would be

$\langle \tau_{off} \rangle = \int t P_{off}(t) dt = \frac{1}{k_{MD}}$ (see section 4.2.2 for the detailed deductions) so it is also

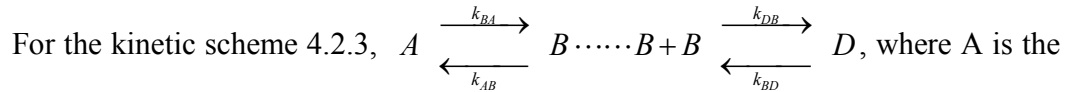
concentration independent. Therefore, it is also rejected. Combining the results from the above two cases, the number of species involved in the trajectories we collected would be more than two according to the off-time variance with concentration.

The kinetic scheme 4.2.3 and 4.2.4 are very similar in that there are two forms of monomers present in the system, one of them is fluorescent and only one of them is linked to the formation of dimers. The only difference between these two schemes lies in that in 4.2.3, the fluorescent form of monomer is linked to the formation of dimers while in 4.2.4, the non-fluorescent form of monomer is directly linked to the formation of dimers. Both kinetic schemes can predict the average on-time to be $1/k_{BA}$ (see section 4.2.3 and 4.2.4 for details). Both the predicted average off-times for these two kinetic schemes show dependence on initial amount (or say, concentration) of MC540 molecules in vesicles. Therefore, we shall discuss the predicted result for each scheme in more detail in the following.



A is the fluorescent form of monomeric MC540, B being the non-fluorescent form and D being the dimeric form of MC540, the average off-time is $\langle t_{off} \rangle = \frac{f_B^{eq}}{k_{AB}} + \frac{f_D^{eq}}{k_{AD}}$. The concentration dependence comes in from f_B^{eq} and f_D^{eq} . However, when estimated with the equilibrium constant for dimerization of MC540 in lipids and our initial conditions, f_B^{eq} or f_D^{eq} shows less than 25% variance (from 0.3 to 0.5 in numerical value). This, when combined with the estimated conventional rate constant^{12, 13} $k_{AB} \sim 1000 \text{ s}^{-1}$ and $k_{AD} \sim$

7500 s⁻¹ (see scheme 3.1), would not give the time scale of average off-times to fall in the range of 10 to 100 ms, as what was observed in our experiments. To get the average off-time to fall in the range from 10 to 100 ms, one would require the kinetic rate constant k_{AD} to become at least 100 times slower (10-100 s⁻¹). This result finds no similar observation in other researchers' attempts to measure the kinetic rate constants. Also, even if the kinetic rate constant k_{AD} were indeed around 10-100 s⁻¹, the concentration variance (0.5 to 0.3, less than two-fold) would not explain a 10 fold decrease of average off-time as seen in our experiments (100 ms to around 10ms). The failure to fit the time scale and concentration dependence of average off-time helps to rule out such kinetic scheme as a reasonable one.



fluorescent form of monomeric MC540, B being the non-fluorescent form of monomeric MC540, and D being the dimeric form of MC540, it would give (see section 4.2.3 for details) an on-time probability density function that follows a single exponential decay

with average on-time $\langle t_{on} \rangle = \frac{1}{k_{BA}}$, an off-time probability density function that is similar

to a doubly exponential decay profile, average off-time to fall within the range 100 to 10 ms and the concentration dependence of the average off-times that fits our experimental results (see figure 4.6 for example). The kinetic scheme, therefore, is not rejected from our analysis using single molecule studies on MC540 bound vesicle intensity-time trajectories. Therefore, the kinetic scheme is retained for our further analysis.

Again, it is entirely possible that more complicated kinetic schemes are involved in our experiments, but what we can gather from a two variable (on and off) intensity trajectory²⁷ would not be able to verify such kinetic scheme (if they are not reducible to simple ones as we have been through) without asserting too many semi-empirical parameters into the analysis. If they are reducible²⁷ to simple kinetic schemes we went through, then only the one as 4.2.3 will prevail in our analysis. On the other hand, Szabo²³⁻²⁸ et al. detailed the statistics involved with the analyses of kinetic models on single molecule fluorescence intensity-time trajectories and should served as basis guideline while performing such kind of analyses.

4.4.2 Polarization dependent studies

As what was mentioned in the introduction section of the chapter, Webb⁸ et al. suggested that MC 540 molecules existed as a monomer in two exchangeable orientations and dimer. The monomers were either in parallel or perpendicular to the membrane surface. The parallel monomers were in equilibrium with dimers. The proposed mechanism was further supported by subsequent studies. However, there had not been any direct photophysical evidence that the two forms of monomers do exist until the work of Amerongen¹⁰ et al came along 2008. By measuring the lifetime of the emitting species (excitation at 570 nm and emission at 580 nm), they resolved two distinct lifetime components for monomer emission: 750 ps and 2 ns. They assigned the long component to monomeric MC540 incorporated deep in the bilayer with perpendicular orientation to the membrane surface and the short component to surface-associated (closer to the edge

of surface) monomers oriented parallel to the membrane. The major emission source of the system under 570 nm excitation was determined to be from perpendicular monomers (to the membrane surface). It can also be reasoned that from the length of the lifetime, the 2 ns component, namely the perpendicular monomers, will envisage a higher emission quantum yield. This could be the emitting source in the kinetic scheme 4.2.3 we analyzed above. Yet, to be more certain what form of monomeric MC 540 is responsible in our system, we performed polarization dependent imaging on MC540 bound GUV and membrane wrapped nanosized silica. The details of the sample preparation and instrumental overview can be found in chapter 2.

(i) Membrane wrapped nanosized silica

The membrane wrapped nanosized silica is chosen for our polarization study due to their rigidity in their spherical shape of the membranes. Therefore, the orientation of the dipole of the emitting species in our system can be well analyzed. The dipole moment of MC540 lies along its long axis on the molecular plane⁸. If the emitting specie in MC540 bound vesicles is perpendicular (to the membrane surface) monomeric MC540, when the system is excited with p-polarized light, one would observe an increase of spots on the cross-section along the x-direction (laboratory coordinate) through the center of the sphere from the edge to the center; when the system is excited with s-polarized light, one would see a decrease of spots on the cross-section along the y-direction (laboratory coordinate) through the center of the sphere from the edge to the center. The predicted situation would reverse if the emitting species is parallel monomeric MC540. In Figure 4.7B, the red curve is the cross-sectional number density along given directions (x or y)

on nanosized silica under p- or s- polarized light excitation while the blue curve is the same object using circularly polarized light excitation. It shows that when compared to the circularly polarized excitation results, the number density of p-polarized excitation shows more centered distribution of spots (red curve, upper-left panel in Figure 4.7B) while the number density of s-polarized excitation shows more spread out distribution of spots (red curve, lower-right panel in Figure 4.7B). Therefore, it coincides with our prediction that the major emitting species in MC540 bound vesicles is perpendicular monomeric MC540. Note that the concentration of MC540 used in the sample resembles that in our PAINT experiment in the last chapter (single molecule condition). This is also the first polarization dependent analysis on super-resolution microscopy studies to the best of our knowledge. It may be a very useful way to analyze orientation distribution of dipole moments of a molecule on a nanoscopic level.

(ii) Giant Unilamellar vesicles

To be more precise on the orientation of the major emitting species in MC540 bound vesicles, we performed another macroscopic level ($[MC540]$ is 1000 times larger than single molecule experiment conditions) polarization measurement. Since dipole moment of MC540 lies along its long axis on molecular plane⁸, linearly polarized light can be used to differentiate which orientation of monomers are responsible for the emission. Only dipole moments that project onto the direction of linearly polarized light can be excited. Therefore, parallel monomers (to the membrane surface), having their dipole moments lining along the circle of cross-section of the GUV, would envisage bright edges on the sides that are parallel to the incident linearly polarized light. If the

perpendicular form (to the membrane surface) of MC540 is responsible for the emission, then the sphere will show brighter fluorescent intensity on the edges that are perpendicular to the direction of the polarization of the incident light. What we observed in Figure 4.8 is that the bright edges shift to the perpendicular direction of the polarization as we vary the direction of the polarization from vertical to horizontal. To be more specific, one can see that on the left panel of the figure 4.8 (A), the bright edges are perpendicular to linearly polarized light (red arrow above the left panel of the image). As the polarized incident linearly polarized light is altered by 90 degree, the bright edges shift to the perpendicular direction of the incident light (see the right panel of the figure 4.8 (B)). Therefore, it is shown that the major emitting species in MC540 bound vesicles is perpendicular monomeric MC540.

Using two different types of samples and two different experimental methods, it leads to the similar conclusion: perpendicular monomeric MC540 is deemed as the major emission species in MC540 bound vesicles.

4.4.3 Further analysis

In the previous section, we conclude the emitting species in our kinetic scheme to be perpendicular monomeric MC540. Now we may include this with the kinetic scheme 4.2.3 for further discussion on the kinetic parameters involved. Now we know in the

kinetic scheme 4.2.3, $A \xrightleftharpoons[k_{AB}]{k_{BA}} B \cdots \cdots B + B \xrightleftharpoons[k_{BD}]{k_{DB}} D$, where A represents

perpendicular monomeric MC540 and B being parallel monomeric MC540. From the

average on-time, one can get k_{BA} for DLPC = 333 s^{-1} , k_{BA} for DMPC = 416.7 s^{-1} , and k_{BA} for DPPC = 400 s^{-1} . The average on-times show no dependence on number of MC540 molecules present in the system. This confirms our previous estimation (previous chapter) that the fluorescent spots stay fluorescent for $\sim 3 \text{ ms}$ (by using the typical kinetic constants to estimate the survival time of M_{\perp} , see Scheme 3.1 for the typical kinetic constants) and switches off. Now it is linked to the perpendicular monomer turning into parallel form of MC540.

For the off-time analysis, we know from previous section (4.2.3) how to simulate the off-time distribution function and hence average off-times for various experimental conditions. The simulated off-time distribution function is displayed in Figure 4.6 (A) and shows a bi-exponential decay. The profile of the distribution function relies on the kinetic constants used in the simulation and only those close to the experimental findings can lead to a bi-exponential decay profile with the sensitivity to amount of MC540 in the system. The average off-times versus the amount of MC540 molecules in the system predicted from the kinetic schemes are also shown in Figure 4.6 (B). It can be seen that only the results from the kinetic scheme 4.2.3 show a number density sensitivity and have average off time decreasing from nearly 100 ms to 10 ms as the number of MC540 increases. This is in parallel to the experimental results in the intensity time trajectories.

From the differential equation
$$\begin{aligned} f_B' &= -k_{AB}f_B - k_{DB}C_T f_B^2 + 2k_{BD}f_D \\ f_D' &= \frac{1}{2}k_{DB}C_T f_B^2 - k_{BD}f_D \end{aligned}$$
, we know the

concentration dependence in the differential equation comes in from the term $k_{DB}C_T$. It remains similar numerical values for all three kinds of lipids so that the off-time

distribution shows bi-exponential decay in the millisecond regime. An interesting feature is that, experimentally, the concentration of the stock solutions of MC540 used for DLPC, DMPC, and DPPC to get the average off-time to fall in 10-100 ms window are 7.5×10^{-11} M, 5×10^{-10} M, and 1×10^{-9} M, respectively. We argue that this is also where it reflects the difference in the kinetic rate constants for various lipids. Since $C_T(\text{DLPC}) < C_T(\text{DMPC}) < C_T(\text{DPPC})$, one can see $k_{DB}(\text{DLPC}) > k_{DB}(\text{DMPC}) > k_{DB}(\text{DPPC})$. Note that there is an equation to link k_{DB} to k_{BD} ($k_{DB} = k_{BD}(1 + k_{AB}/k_{BA})^2 K_d$). It may be possible to estimate all kinetic rate constants involved in the kinetic scheme but it might not be reasonable ones because too many kinetic parameters have been inserted to the simulation of on and off-time distribution from a two variable intensity time trajectories. Therefore, we restrain here to only draw the qualitative conclusion that in different phase of lipids, the decomposition of dimers into parallel monomeric MC540 takes place faster in liquid phase, then liquid/gel mixed phase, and then gel phase. That is to say, dimers of MC540 are more stable in gel phase, then liquid/gel mixed phase, and then liquid phase. The finding here coincide well with the results by other researchers^{2, 11-14}. This is the first experimental analysis to evaluate the stability difference of dimers in different phase of lipids utilizing single molecule kinetic approach to the best of our knowledge.

It is, however, worth noting that conventional photophysical steps might account for the observed intensity time trajectory even though the possibility can be very small. Fluorescence correlation of MC540 in ethanol³⁰ showed that trans-cis isomerization and triplet formation take place on the micro- and nanosecond time scales, respectively, both shorter than the millisecond time frame of our experiments. It is possible that the

isomerization might get slowed down by the lipid, yet it is unlikely to show concentration dependence as is the average off-time measured here.

On the other hand, MC540 molecules may photobleach by forming non-fluorescent states that recover the ground state of the fluorescent MC540 on the millisecond time scale by pathways that depend on the coupling between probes. The power of excitation laser was varied from 4 fold (more than 140 microwatts) of that in the collection of the intensity time trajectory (~35 microwatts) to less than 10 microwatts to see if the average on-time and off-time accordingly. It shows no noticeable change of the average on-time and off-time due to excitation power variation. Also, we collect intensity-time trajectory on the same MC540 bound vesicle continuously for more than eight hours to see if there is a change of the average on-time and off-time due to the decrease of photoactive MC540 molecules after excessive photobleaching, if it does take place in our system. Yet we observed no noticeable change of the average on-time and off-time.

While it cannot be ruled out that the photobleaching might be reversible and non-power dependent, that the isomerization might be slowed down drastically in the lipid or that other photoproducts are involved, the processes that contribute to the intensity-time trajectory would require to have a number of essential features, as discussed above: a millisecond relaxation time, an average off-time that depends on the number density of MC540, and a variation of these properties with the lipid phase. The number density dependence also rules out the process to be as the kinetic scheme we discussed in section 4.2.1 (simple two state equilibration between fluorescent and non-fluorescent states), 4.2.2 (fluorescent monomer forming non-fluorescent dimer and back forth), nor 4.2.4

(fluorescent perpendicular monomeric MC540 changing into and from non-fluorescent parallel monomeric MC540 while fluorescent perpendicular monomeric MC540 directly link to the formation and decomposition of dimers).

4.5 Conclusion

The emitting species is identified to be monomeric MC540 based on the spectra measurement. The number dependence renders the kinetic scheme 4.2.3 to be more reasonable than others. It is then refined by polarization measurement to show it is the perpendicular form of monomers. By using the single molecule intensity-time trajectory studies and polarization dependent imaging measurements, several kinetic schemes were examined and the one prevailed involves the exchanging of fluorescent perpendicular form of monomeric MC540 and non-fluorescent parallel form of monomers while the formation and decomposition of dimers is linked directly to the non-fluorescent parallel form of monomers. By fitting the average on time with the kinetic scheme, we get k_{BA} for DLPC = 333 s^{-1} , k_{BA} for DMPC = 416.7 s^{-1} , and k_{BA} for DPPC = 400 s^{-1} . The formation of parallel monomer from perpendicular monomer takes place around every 3 ms and is not number density dependent. In different lipid, it is also estimated qualitatively that k_{DB} (DLPC) > k_{DB} (DMPC) > k_{DB} (DPPC). It means that the decomposition of dimers are slower in gel phase, there it coincide well with the general understanding that dimers are more stable in gel phase than in liquid phase of lipids^{10, 11, 13}.

This study provides the first evaluation of possible kinetic schemes of MC540 monomer and dimer equilibrium based on single molecule level experiments. It can serve

as an example for examining complicated kinetics in other systems on microscopic level using such intensity-time trajectory approach.

References for Chapter 4:

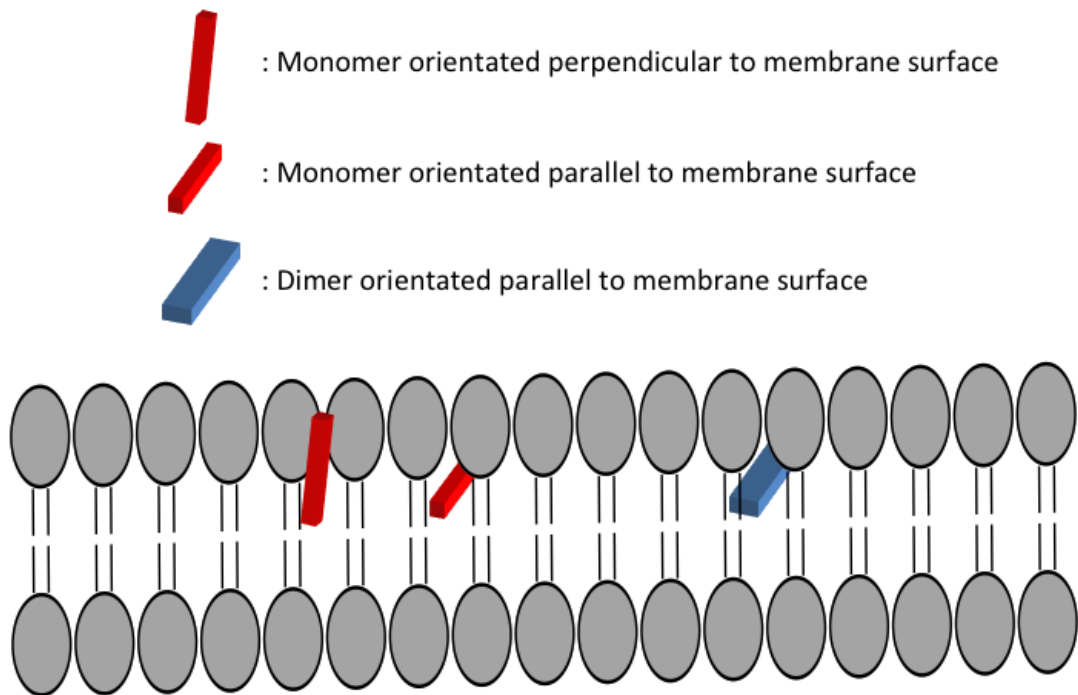
- (1) Aramendia, P. F.; Krieg, M.; Nitsch, C.; Bittersmann, E.; Braslavsky, S. The Photophysics of Merocyanine 540. a Comparative Study in Ethanol and in Liposomes. *Photochem. Photobiol.* **1988**, *48*, 187-194.
- (2) Bernik DL, D. E. Gel State Surface Properties of Phosphatidylcholine Liposomes as Measured with Merocyanine 540. *Biochim Biophys Acta.* **1993**, *1146*, 169-177.
- (3) Yu, H.; Hui, S. Merocyanine 540 as a Probe to Monitor the Molecular Packing of Phosphatidylcholine: A Monolayer Epifluorescence Microscopy and Spectroscopy Study. *Biochimica et Biophysica Acta (BBA) - Biomembranes* **1992**, *1107*, 245-254.
- (4) Williamson, P.; Mattocks, K.; Schlegel, R. A. Merocyanine 540, a Fluorescent Probe Sensitive to Lipid Packing. *Biochim Biophys Acta.* **1983**, *732*, 387-393.
- (5) Salama, G.; Morad, M. Merocyanine 540 as an Optical Probe of Transmembrane Electrical Activity in the Heart. *Science* **1976**, *191*, 485-487.
- (6) Kuo, C.; Hochstrasser, R. M. Super-Resolution Microscopy of Lipid Bilayer Phases. *J. Am. Chem. Soc.* **2011**, *133*, 4664-4667.
- (7) Sharonov, A.; Hochstrasser, R. M. Wide-Field Subdiffraction Imaging by Accumulated Binding of Diffusing Probes. *Proceedings of the National Academy of Sciences* **2006**, *103*, 18911-18916.
- (8) Dragsten, P. R.; Webb, W. W. Mechanism of the Membrane Potential Sensitivity of the Fluorescent Membrane Probe Merocyanine 540. *Biochemistry (N. Y.)* **1978**, *17*, 5228-5240.
- (9) Ehrenberg, B.; Pevzner, E. Spectroscopic Properties of the Potentiometric Probe Merocyanine-540 in Solutions and in Liposomes. *Photochem. Photobiol.* **1993**, *57*, 228-234.

- (10) Krumova, S. B.; Koehorst, R. B. M.; Bóta, A.; Páti, T.; van Hoek, A.; Garab, G.; van Amerongen, H. Temperature Dependence of the Lipid Packing in Thylakoid Membranes Studied by Time- and Spectrally Resolved Fluorescence of Merocyanine 540. *Biochimica et Biophysica Acta (BBA) - Biomembranes* **2008**, *1778*, 2823-2833.
- (11) Bernik, D. L.; Disalvo, E. A. Determination of the Dimerization Constant of Merocyanine 540 at the Membrane Interface of Lipid Vesicles in the Gel State. *Chemistry and Physics of Lipids* **1996**, *82*, 111-123.
- (12) Verkman, A. S.; Frosch, M. P. Temperature-Jump Studies of Merocyanine 540 Relaxation Kinetics in Lipid Bilayer Membranes. *Biochemistry (N. Y.)* **1985**, *24*, 7117-7122.
- (13) Verkman, A. S. Mechanism and Kinetics of Merocyanine 540 Binding to Phospholipid Membranes. *Biochemistry (N. Y.)* **1987**, *26*, 4050-4056.
- (14) Delia Bernik; Elizabeth Tymczyszyn; Marta Edit Daraio; R. Mart ín Negri Fluorescent Dimers of Merocyanine 540 (MC540) in the Gel Phase of Phosphatidylcholine Liposomes. *Photochem. Photobiol.* **1999**, *70*, 40-48.
- (15) Sato, C.; Nakamura, J.; Nakamaru, Y. A Chemometric Approach to the Estimation of the Absorption Spectra of Dye Probe Merocyanine 540 in Aqueous and Phospholipid Environments. *J Biochem* **2000**, *127*, 603-610.
- (16) Chen, P.; Zhou, X.; Shen, H.; Andoy, N. M.; Choudhary, E.; Han, K.; Liu, G.; Meng, W. Single-Molecule Fluorescence Imaging of Nanocatalytic Processes. *Chem. Soc. Rev.* **2010**, *39*, 4560-4570.
- (17) English, B. P.; Min, W.; van Oijen, A.,M.; Lee, K. T.; Luo, G.; Sun, H.; Cherayil, B. J.; Kou, S. C.; Xie, X. S. Ever-Fluctuating Single Enzyme Molecules: Michaelis-Menten Equation Revisited. *Nat Chem Biol* **2006**, *2*, 87-94.

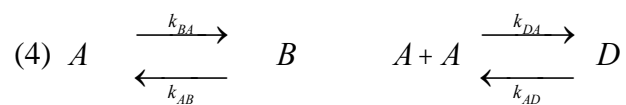
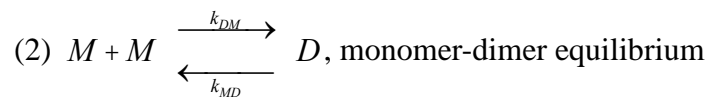
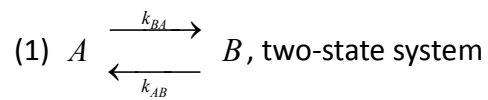
- (18) Barbara, P. F.; Gesquiere, A. J.; Park, S.; Lee, Y. J. Single-Molecule Spectroscopy of Conjugated Polymers. *Acc. Chem. Res.* **2005**, *38*, 602-610.
- (19) Kou, S. C.; Cherayil, B. J.; Min, W.; English, B. P.; Xie, X. S. Single-Molecule Michaelis-Menten Equations. *J Phys Chem B* **2005**, *109*, 19068-19081.
- (20) Lu, H. P.; Xun, L.; Xie, X. S. Single-Molecule Enzymatic Dynamics. *Science* **1998**, *282*, 1877-1882.
- (21) Jianshu, C. Event-Averaged Measurements of Single-Molecule Kinetics. *Chemical Physics Letters* **2000**, *327*, 38-44.
- (22) Gao, F.; Mei, E.; Lim, M.; Hochstrasser, R. M. Probing Lipid Vesicles by Bimolecular Association and Dissociation Trajectories of Single Molecules. *J. Am. Chem. Soc.* **2006**, *128*, 4814-4822.
- (23) Berezhkovskii, A. M.; Szabo, A.; Weiss, G. H. Theory of Single-Molecule Fluorescence Spectroscopy of Two-State Systems. *J. Chem. Phys.* **1999**, *110*, 9145-9150.
- (24) Berezhkovskii, A. M.; Szabo, A.; Weiss, G. H. Theory of the Fluorescence of Single Molecules Undergoing Multistate Conformational Dynamics. *J Phys Chem B* **2000**, *104*, 3776-3780.
- (25) Gopich, I. V.; Szabo, A. Statistics of Transitions in Single Molecule Kinetics. *J. Chem. Phys.* **2003**, *118*, 454-455.
- (26) Gopich, I.; Szabo, A. Theory of Photon Statistics in Single-Molecule Förster Resonance Energy Transfer. *J. Chem. Phys.* **2005**, *122*, 014707.
- (27) Flomenbom, O.; Klafter, J.; Szabo, A. What can One Learn from Two-State Single-Molecule Trajectories? *Biophys. J.* **2005**, *88*, 3780-3783.

- (28) Gopich, I. V.; Szabo, A. Theory of the Statistics of Kinetic Transitions with Application to Single-Molecule Enzyme Catalysis. *J. Chem. Phys.* **2006**, *124*, 154712-21.
- (29) Dodin, G.; Aubard, J.; Falque, D. Thermodynamic and Kinetic Studies of the Interaction of Merocyanine 540 with Hydrophobic Aggregates. 1. Binding of Merocyanine 540 to Sodium Dodecyl Sulfate Micelles. *J. Phys. Chem.* **1987**, *91*, 1166-1172.
- (30) Widengren, J.; Seidel, C. A. M. Manipulation and Characterization of Photo-Induced Transient States of Merocyanine 540 by Fluorescence Correlation Spectroscopy. *Phys. Chem. Chem. Phys.* **2000**, *2*, 3435-3441.

Schemes for Chapter 4:



Scheme 4.1. Illustration of relative position and orientation of MC540 perpendicular monomers (to membrane surface), parallel monomers, and dimers in a membrane lipid bilayer.



Scheme 4.2. Proposed kinetic schemes for the intensity-time trajectory for MC540 bound vesicles. A and M represent the fluorescent species (monomers) in MC540 bound vesicles, B represents non-fluorescent one, and D represents dimers of MC540.

Figures for Chapter 4:



Figure 4.1. Typical fluorescence images of MC 540 bound vesicles on a glass surface. The size of the image is 5 μm x 5 μm .

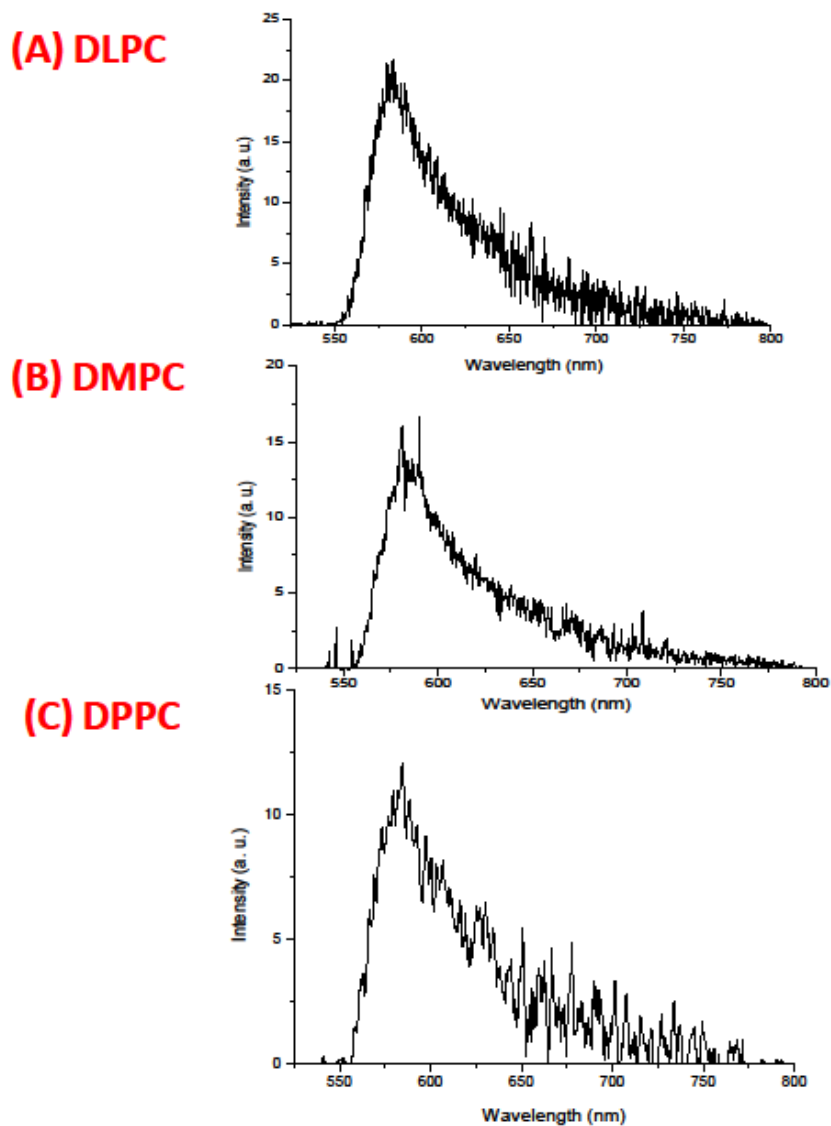


Figure 4.2. Bulk fluorescence spectra of MC540 bound (A) DLPC- (B) DMPC- (C) DPPC- vesicle on a glass surface. The spectra are recorded on a confocal microscope with monochromator and CCD camera (see chapter 2 for instrumental overview).

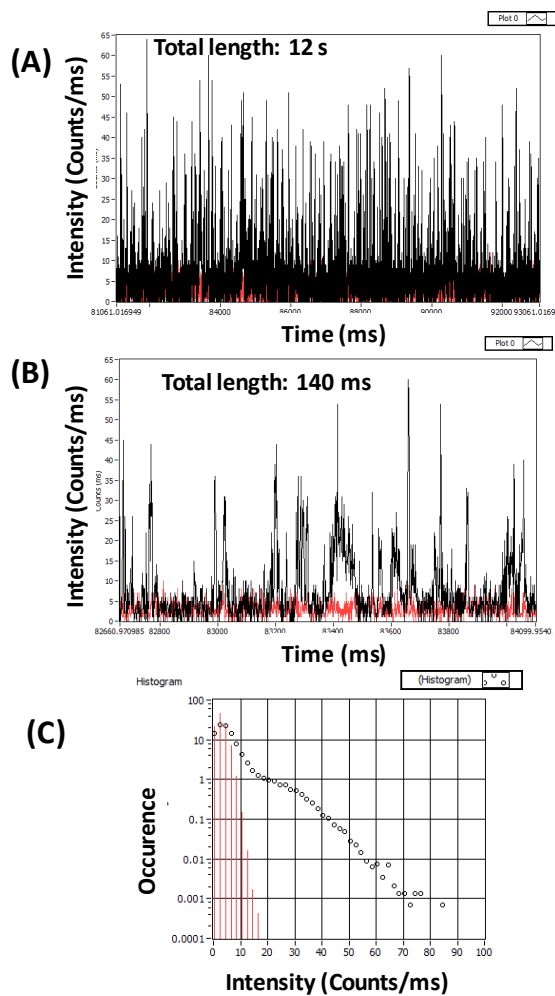


Figure 4.3. Typical fluorescence intensity-time trajectory on a MC540 bound DMPC vesicle with different length. (A) Trajectory length: ~12 s (B) Trajectory length: ~140 ms (extracted from (A)). The red curve shows background signal when no excitation is applied to the system for comparison. (C) The corresponding count rate distribution (black circle) is calculated based on the intensity-time trajectory in (A). The red lines represent background signal level. The concentration of MC540 used is ~1 nM.

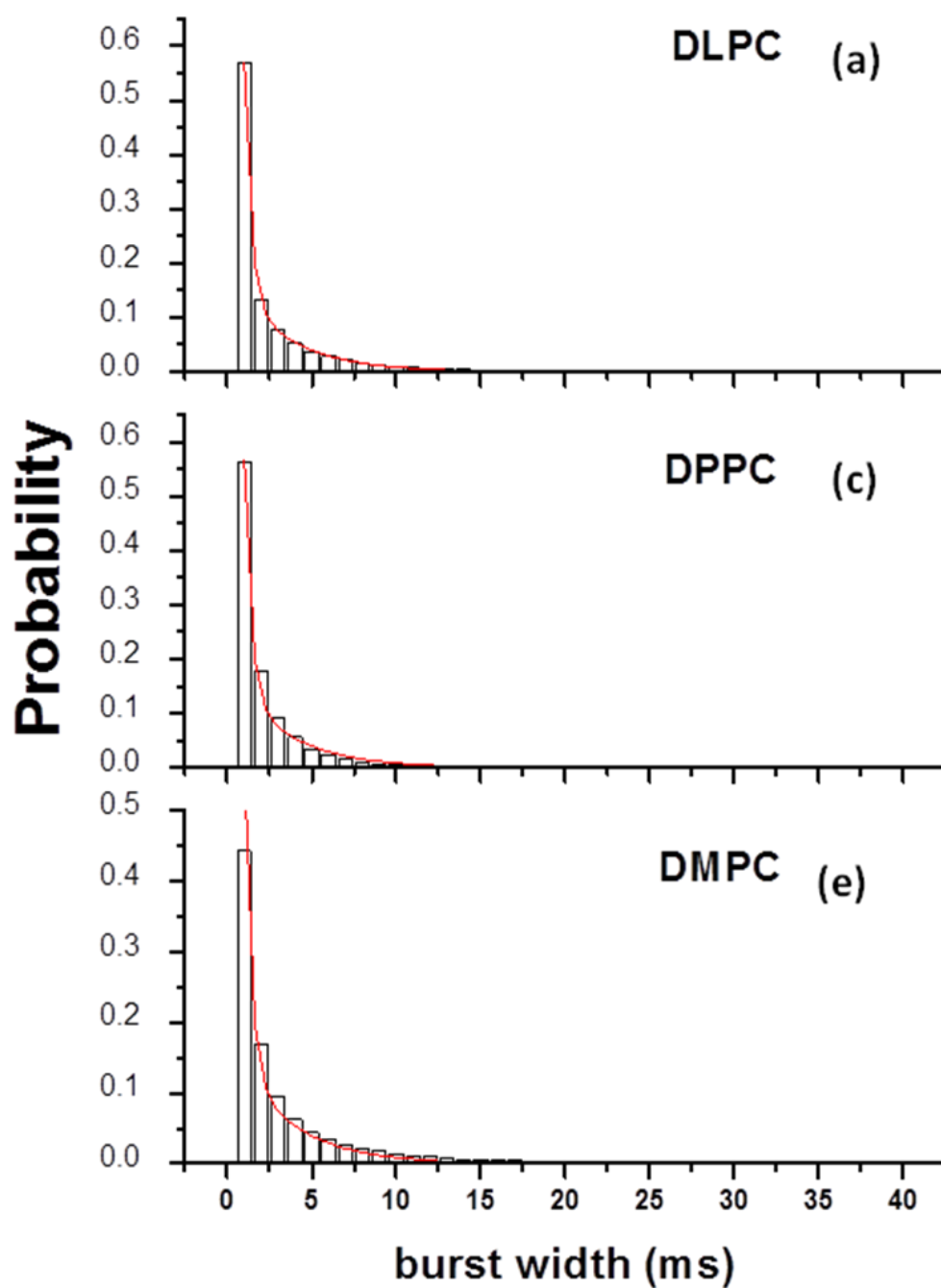


Figure 4.4. Probability distributions of the width of fluorescence bursts from over 250 MC540 bound (a) DLPC- (c) DMPC- (e) DPPC- vesicles. The red curve indicates a single exponential decay fits to the data.

(Continued)

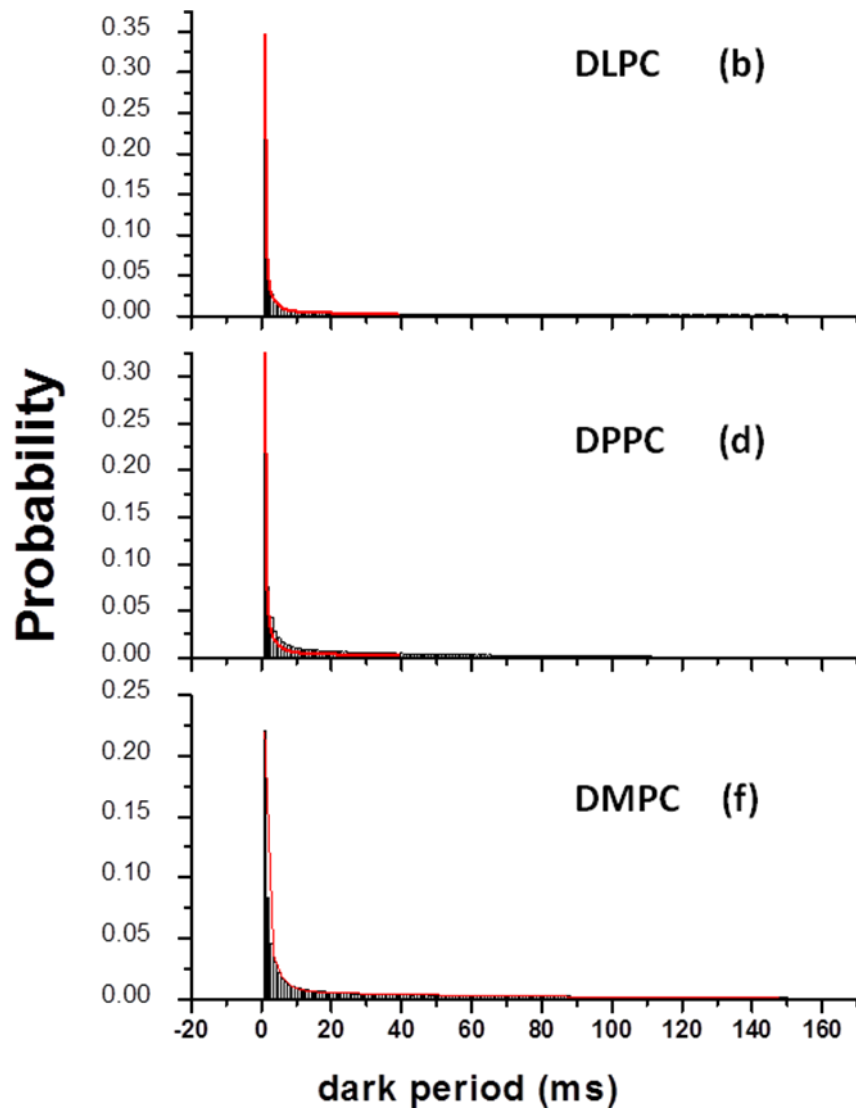


Figure 4.4(continued). Probability distributions of the width of drak periods from over 250 MC540 bound (a) DLPC- (c) DMPC- (e) DPPC- vesicles. The red curve indicates a double exponential decay fits to the data.

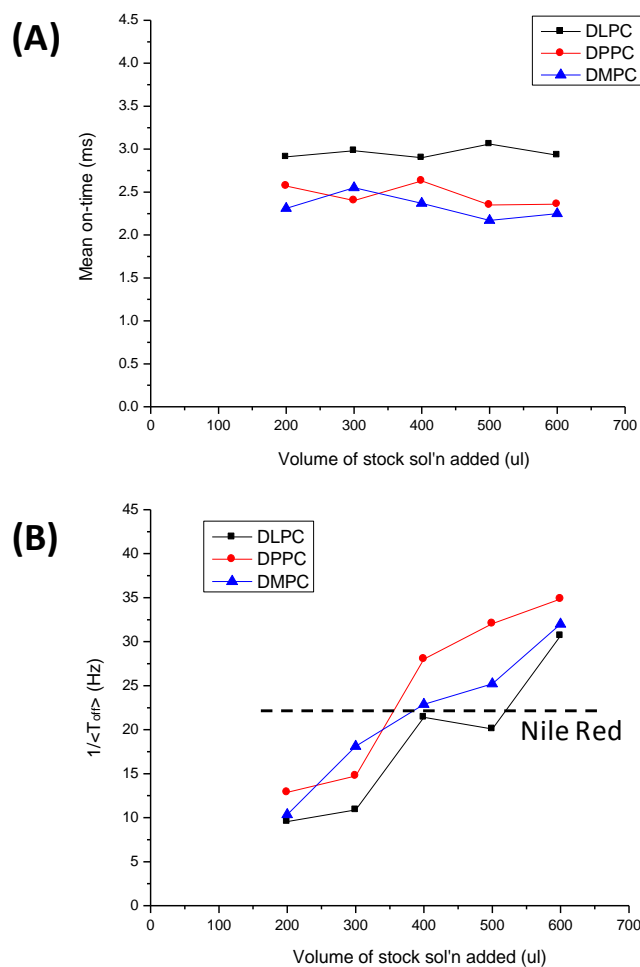


Figure 4.5. (a) Mean on-time for various volumes of MC540 stock solution added in the lipid vesicles of DLPC, DPPC, and DMPC. (b) Mean off-time frequency for various volumes of MC540 stock solution added in the lipid vesicles of DLPC, DPPC, and DMPC. The dashed line denotes the case for Nile Red bound DMPC vesicles and is shown here for comparison.

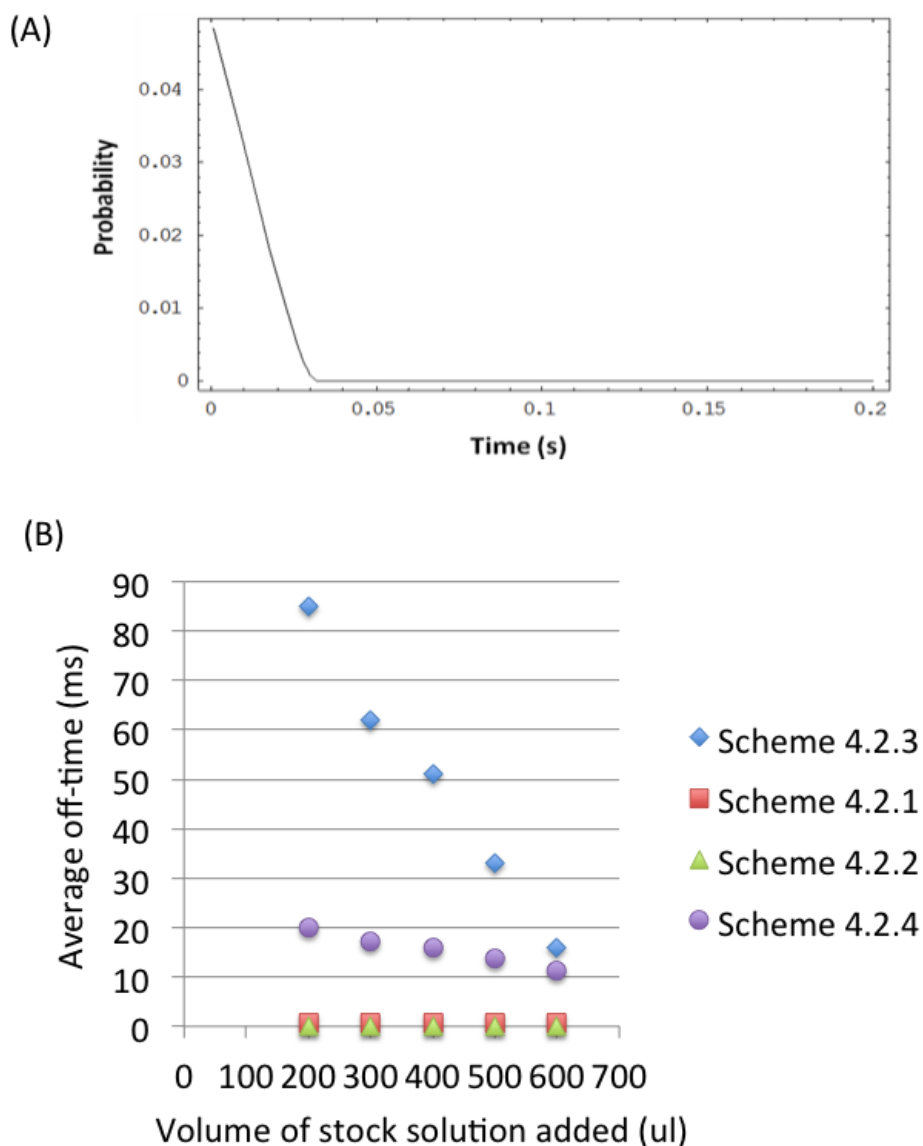


Figure 4.6. (A) Typical simulated off-time probability distribution using the differential equations from the kinetic scheme 4.2.3. The parameters used for the simulations are $k_{AB} = 1800 \text{ s}^{-1}$, $k_{DB}C_T = 20000$, $K_d = 4 \times 10^3 \text{ M}^{-1}$, $k_{AB}/k_{BA} = 6$, and $P_B^{eq} = 0.8$ and $P_D^{eq} = 0.3$. (B) Predicted average off-time versus amount of MC540 molecules in lipid bilayers from various kinetic scheme.

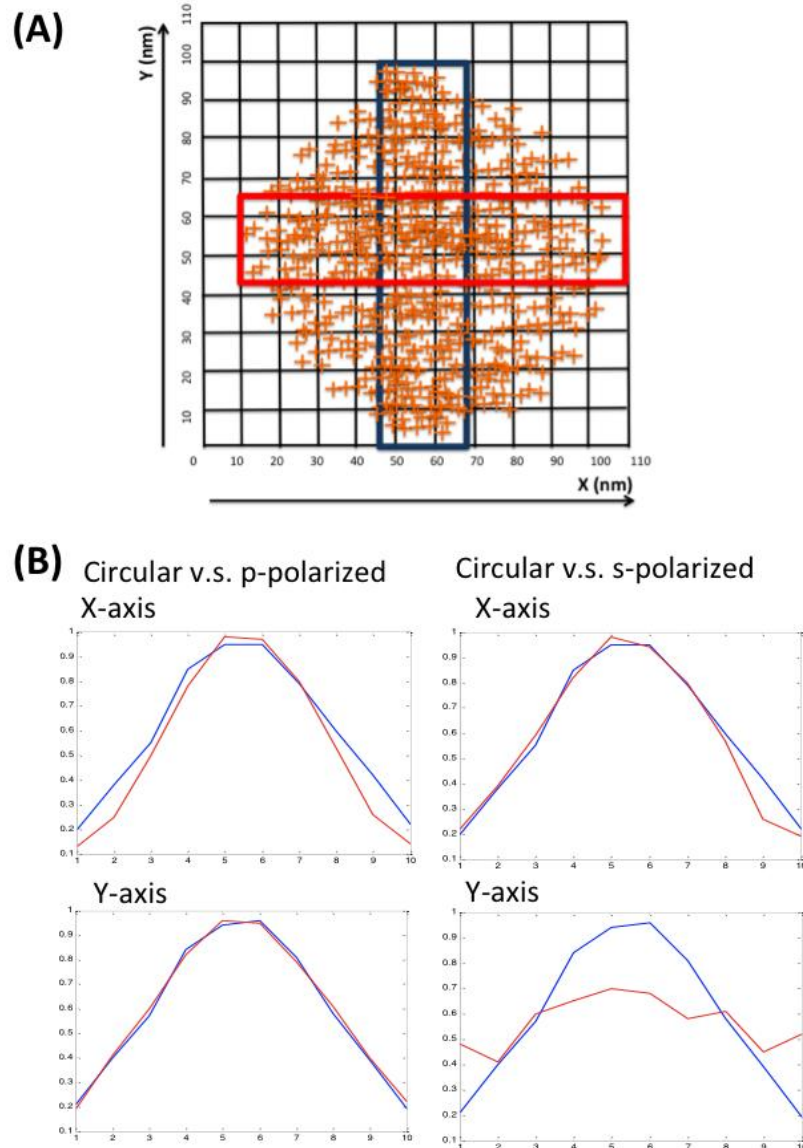


Figure 4.7. (A) Typical synthesized polarization dependent PAINT images (p-pol) of nanosized lipid bilayer wrapped silica (100 nm in size). Each cross indicates a presence of a fluorescent spot. The rectangular box represents the region that is extracted to get the number density distribution of spots along either x- (red) or y-(blue) direction across the sphere to form analysis in (B). The dimension of the

image (A) is around 110 nm by 110 nm. (B) Comparison of the number density distribution along either x- or y- axis across the nanosized silica (divided into 10 bins) with circularly polarized (blue curves in all panels), p-polarized (red curves on the left panels), or s-polarized light (red curves on the right panels). The red or blue box in (A) indicates the regions cropped to yield the number density distribution. Each box is further divided into 10 bins (each bin is around 25 nm by 10 nm in dimension) to perform the histogram analysis.

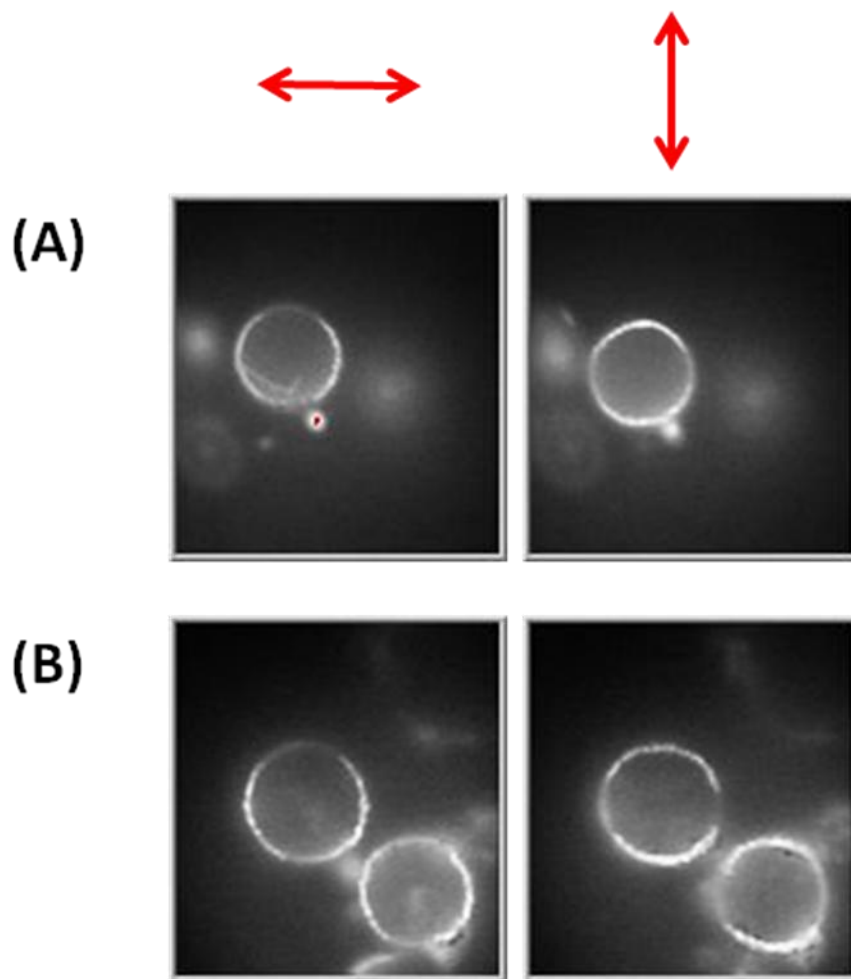


Figure 4.8. Typical polarization dependent fluorescent images of DLPC GUVs. The arrow indicates the direction of the linear polarization of the incident light. The dimension of each image is around $30\mu\text{m}$ by $30\mu\text{m}$. (A) and (B) are collected from different regions.

Chapter 5 Conclusion

Super-resolution microscopy has become a powerful tool to study biological samples with ultra-high resolution to see beyond diffraction limit. The PAINT method, one of the super-resolution imaging methods, relies on the interaction of single molecule fluorophores and their interaction with the immediate surroundings. The control of thermal reaction rates is used to enable the switching between bright and dark states, and hence the localized single molecule spots form the synthetic image. In the thesis, the PAINT method is integrated with a phase sensitive probe, MC540 to image nanoscale phase separation of lipids. Such approach can serve as a strategy for further application to image phase separation phenomena in biological samples, like lipid rafts on cell membranes. To better understand the underlying kinetics involved in the MC540 bound lipids, we performed a series of analyses on the fluorescent intensity time trace of MC540 bound vesicles of various lipid phases. The kinetic scheme (see 4.2.3), which involves the interchange of two forms of MC540 monomers, one parallel to the lipids, and the other one perpendicular, and only the parallel form is directly linked to the formation and discomposition of dimers, is validated in our study.

The goal of visualizing the nanoscopic sphingolipid/cholesterol-rich domain in natural membranes has stimulated numerous investigations either by direct visualization or indirect inferences from the tracking of diffusing probes. Nevertheless visualization or systemization of such domains (rafts), assumed to vary from tens to several hundred

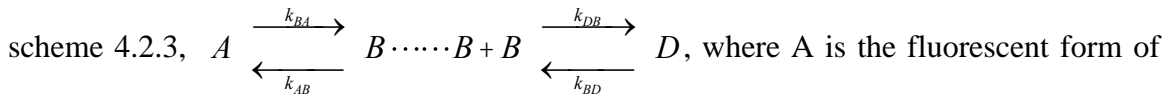
nanometers in cell membranes, remains challenging. In this work, the “points accumulation for imaging in nanoscale topography” (PAINT) method, which has sub-diffraction resolution, is combined with a lipid phase-sensitive probe merocyanine 540 (MC540 hereafter), to illustrate that nanoscale phase separations on a supported lipid bilayer (SLB) can be visualized by this method.

In chapter 3, it was shown that the PAINT method of super-resolution imaging using the dye MC540 is useful for imaging phase domains in binary lipid bilayers. The monomer-dimer dynamic equilibrium of MC 540 in lipids is essential to the repopulation of photobleached monomers. The distinction between lipid phases arises because the average number density of fluorescent monomeric MC 540 molecules in the liquid phase of the supported lipid bilayers is ca. 3 times larger than that in gel phase. The synthetic image (the PAINT image) was obtained by superimposing all fitted single molecule points and applying pseudo color mapping, thereby revealing phase separation of DOPC:DPPC 3:1 at subdiffraction resolution. Many nanoscopic domains of the gel phase were seen. The extension of this method to other binary or ternary lipid model or natural systems provides a promising new super-resolution strategy.

It has long been considered that the monomeric form of MC540 resides close to the lipid head group, and that the monomers are in large measured perpendicular to the membrane surface (M_{\perp}). To form an anti-parallel dimer, the monomers have to migrate to a deeper position in the membrane and reorient into parallel forms of MC540 (M_{\parallel}). The dimers (M_2 or D) are parallel to membrane surface and in a deep position compared to the perpendicular monomers. It is therefore quite intuitive for one to reason that

perpendicular monomer of MC540 is the emitting species that forms the on states of the bursts we observed in the imaging section (chapter 3) of the thesis, while the dimers are present during the off times as the bursts disappear. However, since MC540 as a probe combined with the PAINT method serves as the first example for phase sensitive super-resolution microscopy, it is worthwhile to gather more concrete evidence for the emitting species and the underlying kinetics leading to the on and off states. Here we resort to kinetic studies on single molecule level and polarization dependent imaging to achieve the goal.

Single molecule intensity trajectory collection has been a powerful tool to see beyond the ensemble averaging, and therefore enable access to detailed information in various ways: (1) a probability density distribution function for an experimental observable, instead of a single, mean value, is provided; (2) static and dynamic heterogeneity of the observables can be differentiated; (3) statistically rare events, like transitions between different functional states, can be explored; and (4) possible kinetic schemes can be evaluated through analysis of these distribution functions. In chapter 4, four potential kinetic schemes that may be responsible for the turning on and off for the fluorescent spots in MC540 bound lipid membranes are proposed and the corresponding on and off time distribution functions are evaluated. They are compared with those obtained from the intensity time trajectories of MC540 bound vesicles. For the kinetic



monomeric MC540, B being the non-fluorescent form of monomeric MC540, and D

being the dimeric form of MC540, it would give (see section 4.2.3 for details) an on-time probability density function that follows a single exponential decay with average on-time

$\langle t_{on} \rangle = \frac{1}{k_{BA}}$, an off-time probability density function that is similar to a doubly

exponential decay profile, average off-time to fall within the range 100 to 10 ms and the concentration dependence of the average off-times that fits our experimental results. The kinetic scheme, therefore, is not rejected from our analysis using single molecule studies on MC540 bound vesicle intensity-time trajectories. Therefore, the kinetic scheme is retained for our further analysis. In section 4.4.2, the polarization dependent studies confirmed that perpendicular form of monomeric MC540 is the emitting species.

By using the single molecule intensity-time trajectory studies and polarization dependent imaging measurements, several kinetic schemes were examined and the one that prevailed involves the exchanging of fluorescent perpendicular forms of monomeric MC540 and non-fluorescent parallel forms of monomers, while the formation and decomposition of dimers is linked directly to the non-fluorescent parallel form of monomers. By fitting the average on time with the kinetic scheme, we get k_{BA} for DLPC = 333 s⁻¹, k_{BA} for DMPC = 416.7 s⁻¹, and k_{BA} for DPPC = 400 s⁻¹. The formation of parallel monomer from perpendicular monomer takes place around every 3 ms and is not number density dependent. For different lipids, it was estimated qualitatively that k_{DB} (DLPC) > k_{DB} (DMPC) > k_{DB} (DPPC). It means that the decomposition of dimers are slower in gel phase, there it coincide well with the general understanding that dimers are more stable in gel phase than in liquid phase of lipids.

This study provides the first evaluation of possible kinetic schemes of MC540 monomer and dimer equilibrium based on single molecule level experiments. It can serve as an example for evaluating complicated kinetics in other systems on microscopic level using such intensity-time trajectory approach. Instead of affirming a certain kinetic scheme by fitting probability distribution function of on- and off- times with pre-assumed kinetic schemes, here proposed kinetic schemes are rejected if the projected probability distribution functions (from modeling) are not in line with the ones from experimental observations.